Doctor of Philosophy

Routing Protocols in Opportunistic Mobile Social Networks Based on Human Behavior Pattern Detection

The Graduate School of the University of Ulsan

Department of Electrical, Electronic and Computer Engineering

DUONG VAN ANH DAT

Routing Protocols in Opportunistic Mobile Social Networks Based on Human Behavior Pattern Detection

Supervisor: Prof. Seokhoon Yoon

A Dissertation

Submitted to
the Graduate School of the University of Ulsan
In partial Fulfillment of the Requirements
for the Degree of

Doctor of Philosophy

by

Duong Van Anh Dat

Department of Electrical, Electronic and Computer Engineering

University of Ulsan, Korea

June 2022

Routing Protocols in Opportunistic Mobile Social Networks Based on Human Behavior Pattern Detection

This certifies that the thesis of Duong Van Anh Dat is approved by:

Committee Chair: Prof. Myung-Kyun Kim

Committee Member: Prof. Jin-Ho Chung

Committee Member: Prof. Daehwan Kim

Committee Member: Prof. Dae-Young Kim

Committee Member: Prof. Seokhoon Yoon, *Adviser*

Department of Electrical, Electronic and Computer Engineering

University of Ulsan, Korea

June 2022

Dedicated to

My beloved wife, son, parents, parents-in-law, sisters, and brothers, …

Acknowledgments

First, I would like to express my heartfelt gratitude to my advisor, Prof. Seokhoon Yoon of the Department of Electrical, Electronic and Computer Engineering, University of Ulsan, for his excellent guidance and support throughout my studies. As a result of his critical comments and suggestions, I have learned how to do successful research and have accumulated a wealth of valuable knowledge. Without his advice and guidance, none of my work would have been possible.

Additionally, I would like to express my gratitude to the committee members for reviewing my thesis and providing insightful comments that assisted me in improving the quality of my thesis.

I would like to thank my parents, parents-in-law, sisters, brothers, and friends for their encouragement and inspiration during the period of my studies. I also thank my research colleagues in the Advanced Mobile Networks and Intelligence Systems Laboratory, who always give me useful comments and fun memories.

Last but not least, I thank my beloved wife and son for their endless love, patience, and support during my stay at the University of Ulsan.

Abstract

With the increasing number of smart device users, a network architecture called opportunistic mobile social network (OMSN) is gaining attention. OMSNs have been used in a variety of applications, such as environmental monitoring, intelligent transportation systems, and public safety. However, routing in OMSNs is a challenging problem due to the frequent disconnection between nodes and the absence of paths from the source to the destination. It results in a complex topology and a low packet transmission success rate. Therefore, this thesis studies routing protocols in OMSNs. Specifically, a human mobility model that generates human movements is first designed. Then, a temporal social interaction-based routing protocol is developed, and the proposed human mobility model is used to validate the performance of this routing protocol. Finally, we extend our work by studying a human location prediction model and proposing a human location prediction-based routing protocol.

First, human movement patterns are important for validating the performance of routing protocols. Several traces of human movements in real life have been collected. However, collecting data about human movements is costly and time-consuming. Moreover, multiple traces are demanded to test various network scenarios. As a result, a lot of synthetic models of human movement have been proposed. Nevertheless, most of the proposed models were often based on random generation, and cannot produce realistic human movements. Although there have been a few models that tried to capture the characteristics of human movement in real life, those models still cannot reflect realistic human movements due to a lack of consideration for social context among people. To address those limitations, we propose a novel human mobility model called the social relationship−aware human mobility model (SRMM), which considers social context as well as the characteristics of human movement (e.g., flights, inter-contact times, and pause times following the truncated power-law distribution). SRMM partitions people into social groups by exploiting information from a social graph. Then, the movements of people are determined by considering the distances and social relationships.

In the second part of this work, we design a routing algorithm called the temporal social interactions-based routing protocol (TSIRP) for solving challenges in OMSNs. First, we focus on the temporal context of social interactions. Specifically, at a certain time of the day, a person usually interacts with specific people (e.g., workers usually meet co-workers during

working hours; students usually meet their classmates during class). Based on temporal social interactions between nodes, potential forwarding metrics are proposed and calculated for each time of the day to make forwarding decisions. Second, we propose a new scheme to control the message spreading rate, which allows achieving a balance between delivery latency and overhead ratio. In addition, an analytical model is also designed using an absorbing Markov chain to estimate the performance of TSIRP. SRMM is used to generate human movements for evaluating the performance of TSIRP.

In the third part of this work, a specific scenario for transmitting data in urban sensor networks is studied and a human location prediction-based routing protocol (HLPRP) is proposed for this network model. Specifically, a human location prediction (HLP) model is designed to estimate the location of mobile nodes. The proposed HLP model is based on a recurrent neural network with long short-term memory cells. The movement history of each person is used in the HLP model to predict their future locations. Then, using predicted location information from the HLP model, packet delivery predictability is obtained. Packet delivery predictability represents the possibility that a node will deliver a packet to its destination and is used to select optimal relay nodes to maximize the packet delivery ratio, minimize the packet delivery cost, and reduce delivery latency. In addition, the proposed routing protocol also considers social strength for relay selection.

Simulations on a synthetic map and a real road map are considered to evaluate SRMM. The results of SRMM are compared with a real trace and other synthetic mobility models. The obtained results indicate that SRMM is consistently better at reflecting both human movement characteristics and social relationships. Then, using the generated human movements from SRMM, we conduct experiments with different parameters to validate TSIRP. Simulations on real traces (e.g., UB datasets) are used to evaluate HLPRP. The evaluated results show that TSIRP and HLPRP can achieve better performance than existing routing protocols.

Contents

List of Figures

List of Tables

Chapter 1

Introduction

1.1 Human Movement Pattern

Human movement patterns greatly affect the performance of various wireless networks, such as opportunistic mobile social networks (OMSNs), which rely on human movement for pairwise contacts between two communicating devices. Therefore, in order to fully validate such networks, various realistic human movement patterns should be considered. Unfortunately, collecting real-life human movements in various situations is highly time consuming and costly, and it may be infeasible at a very large scale (e.g., citywide or countrywide). That leads to a limited number of available real traces. Therefore, synthetic models for human movement generation are mostly used.

As a result, a lot of synthetic models have been proposed. For instance, the Markovian waypoint model [1] and the random direction model [2] have been used for a long time. A major disadvantage of those models is that they are based on purely random generation of human movement. Thus, the context in real life (e.g., people usually visit their friends, and the places people visit are related over days) were not considered. That causes significant disagreement between the output of mobility models and human movements in the real world.

Recently, several studies have seriously analyzed real human movement traces and found interesting human movement characteristics where flights, inter-contact times (ICTs), and pause times follow truncated power-law distributions [3, 4]. Inspired by these studies, a few mobility models, such as the self-similar least action walk (SLAW) [5] and the working day movement model [6], studied to capture human movement characteristics. However, such models did not consider the social context among people. Therefore, they could not fully

reflect human movement in real life.

Social relationships among people are an interesting way to construct mobility models (e.g., community-based mobility model (CMM) [7], home-cell community-based mobility model (HCMM) [8]). Such models consider social context. For example, people prefer to visit places where many of their friends are staying. However, those models did not take into account human movement characteristics, such as flights, ICTs, the radius of gyration, and pause time distributions. Additionally, selecting the destinations of people is only affected by their social ties without considering important contexts (e.g., in real life, the places an individual visits during different day trips are correlated, and people tend to visit nearby places). For those reasons, such models could not reflect realistic human movement.

To reflect realistic human movement, a mobility model needs to consider both human movement characteristics and the social context between people.

1.2 Proposed Human Mobility Model

In order to address the limitations in existing models and reflect realistic human movements, we propose a novel human mobility model called the social relationship−aware human mobility model (SRMM), which takes into account social relationships among people and human movement characteristics.

Specifically, SRMM considers the characteristics of human movements in terms of flights, ICTs, the radius of gyration, and pause-time distributions. A flight is defined as a Euclidean distance between two consecutive spots visited by an individual. Spots are the geographic positions in which a person stays for longer than a certain amount of time. Studies have shown that the distribution of flights follows truncated power-law distributions [3, 4]. ICT represents the time elapsed between two successive contacts for a given pair of people. Freeman investigated real-life human movements and reported that the ICTs of people in real life can be reproduced in truncated power-law distributions [9]. The next characteristic is the radius of gyration, which indicates the spatial extent of a person's trajectory during an observation period. According to work by Gonzalez et al. [3], the radius of gyration can also be modeled by truncated power-law distributions. Finally, pause time (the sojourn time of a person in one spot) was analyzed [4, 10]. The obtained results demonstrated that pause times during movement have truncated power-law distributions. SRMM captures the truncated power-law distributions of flights, ICTs, the radius of gyration, and pause times.

In SRMM, the social characteristics of humans are also considered. Our model takes

a social graph as input, which represents the relationships among people, followed by a clustering algorithm that partitions people into social groups. Each social group represents a community in the real world, such as a family, a class, or a football team. Then, spots to be visited by people are generated and grouped into places, i.e., a place (e.g., a mall) consists of multiple spots (e.g., clothing stores, the cafeteria, and restrooms). We use the observation that people in the same community usually visit similar places. For instance, the members of a football team often visit the same places, such as the stadium, the canteen, and the dressing rooms. SRMM chooses a group of frequently visited places for a social group. As a result, the people in a social group will have the same frequently visited places. Then, each person chooses frequently visited spots from frequently visited places.

Our model also considers scenarios where people sometimes visit a new place (different from places other members in the same social group visited) by adding randomly visited spots for each person at the beginning of each day. The frequently visited spots and the randomly visited spots for a person are defined as candidate spots.

During daily trips, each person selects destinations from his/her candidate spots. To select destinations, human movement properties and social relationships are considered. In SRMM, a person selects a destination based on the distance from the person's current location and the number of social acquaintances they have (i.e., people from the same social group) in those places. Specifically, a place that is a shorter distance away and that accommodates a larger number of social acquaintances has a higher probability of being visited. The detailed description of SRMM will be presented in Chapter 3.

1.3 Routing Protocol in Opportunistic Mobile Social Networks

In recent years, because of the evolution of mobile communication technologies, people can easily access a lot of useful information through smart devices such as smartphones and tablets, which gradually became an integrated part of people's daily life. This strongly promoted the development of opportunistic mobile social networks (OMSNs) [11–13], which consist of human-carried mobile devices that exchange data with each other via short-range wireless communications. The major advantage of OMSNs is that it requires a low cost and does not rely on any infrastructure. In the application of opportunistic mobile social networks [14, 15], user experience is the most important. However, the connection between nodes is intermittent due to nodes' mobility in OMSNs, and delivering messages becomes a challenging issue. Therefore, a lot of routing protocols have been proposed to address this

issue.

A lot of routing protocols for transferring data between nodes in OMSNs have been studied [16–22]. For example, several routing methods use the flooding strategy [16, 17]. However, with the flooding strategy, messages are immediately spread when there are contacts between nodes. As a result, those routing protocols consume a lot of resources and have a high network overhead ratio. To minimize overhead, the number of replications was limited in [18]. Nevertheless, this routing protocol did not take into account optimal relay selection. Therefore, low mobility nodes can be selected to forward messages, resulting in a low packet delivery ratio and long delivery latency. In [19–21], nodes that recently encountered the destination are preferred for selection as relay nodes. However, in a real context, two individuals may often meet in the present moment, but their next meeting may occur in the distant future. For example, family members frequently interact in the morning but do not meet until the evening. As a result, the optimal relay nodes may not be chosen, and those routing protocols may not achieve high network performance.

To address limitations in the existing routing protocols in relay selection, which causes high delivery cost (DC), a long packet delivery latency (PDL), and a low packet delivery ratio (PDR), we first design a routing algorithm based on the temporal social interactions. Then, we propose a routing protocol based on human location prediction.

1.4 Proposed Routing Protocols

1.4.1 Temporal Social Interactions-Based Routing Protocol

In this section, we introduce the temporal social interactions-based routing protocol (TSIRP). TSIRP is considered with general scenarios for exchanging messages between nodes in OMSNs. Under TSIRP, the movement history of the nodes is looked at, and temporal social interactions are used to get possible forwarding metrics (PFMs). These metrics are then used to choose relay nodes. Specifically, for each time of day, the chances that two nodes will meet are estimated based on information from the past when they met each other. Then, based on the encounter probabilities and inter-contact time between nodes, three PFMs are determined, which are the expected delivery delay, the number of time slots to satisfy the meeting probability condition, and the mean value of inter-contact time.

Moreover, under TSIRP, the message spreading rate is controlled based on the state of the message in order to achieve a balance between PDL and DC. Specifically, when

a message has just been generated, it should be quickly spread to increase the number of copies in the network, which leads to lower latency. After the message has spread enough, the message spreading rate should be decreased to reduce DC. Based on the forwarding token and the residual lifetime of the message, in our work, a metric called the spreading rate control value is proposed to adjust the message spreading rate. Specifically, when the forwarding token is large (i.e., only a few copies are in the network) and the residual lifetime of a message is long, the message is quickly forwarded to neighboring nodes via broadcast without performing relay selection. When the forwarding token is low (i.e., sufficient copies are in the network) and the residual lifetime of the message is short, the node only forwards the message to selected relay nodes, i.e., the message spreading rate is decreased. Chapter 4 will describe TSIRP in details.

1.4.2 Human Location Prediction-Based Routing Protocol

In this section, we first introduce a network model based on OMSNs, and then the human location prediction-based routing protocol (HLPRP) that is proposed for routing messages in this network is briefly summarized.

Specifically, mobile crowdsensing (MCS)-based urban sensor networks are considered. This model includes a server center, edge nodes, sensors, and mobile users. It can be used in a variety of urban-sensing applications, such as environmental monitoring [23,24], intelligent transportation systems [25,26], and public safety [27]. Mobile users collect data using sensors in their smart devices. Sensors are deployed in certain places to capture data such as air pollution, radioactivity, noise level, and humidity. Edge nodes are placed in particular locations to gather and preprocess data from sensors and mobile users. Then, edge nodes send processed data to the server center, where it is used for a variety of applications. The server center communicates with edge nodes using an infrastructure-based wired or wireless network. For communication between other components (i.e., edge nodes, sensors, and mobile users), the wireless interfaces (e.g., Bluetooth 5.0) are used without the need for an infrastructure network. The primary benefit of this network is that it is cost-effective. However, that requires an effective routing protocol to transfer data between edge nodes, sensors, and mobile users.

In this thesis, we also propose a human location prediction (HLP)-based relay selection model that uses a recurrent neural network (RNN) with long short-term memory (LSTM) cells [28]. RNNs have emerged as a potential model for processing sequential data in a

variety of applications, such as time-series prediction, video tagging, speed recognition, and generating image descriptions. However, RNNs suffer from both gradient vanishing and gradient explosion problems with long sequences of input. Therefore, we use LSTMs to overcome the problem. A RNN with LSTM cells contains states that enable them to process variable-length sequences of input. In other words, those states are capable of capturing historical information from an arbitrary length of the context window. In the proposed HLP model, the movement histories of mobile users in current and previous time slots (e.g., mobile users' identities, mobile users' positions, the time slot of the day, the day of the week) are used to predict their positions in the next several time slots with high accuracy. Note that edge nodes are deployed in specific locations in MCS-based urban sensor networks, and packet destinations are among the edge nodes. Packet delivery predictability is calculated based on the probability that a mobile node will visit an edge node's position. A mobile node with a high probability of meeting an edge node during a certain time slot has a high value for packet delivery predictability to that edge node. Packet delivery predictability represents the possibility that a node will deliver a packet to its destination.

In addition, the social relationships between nodes are taken into account based on their movement histories. Two nodes have high social strength if they interact frequently over a long period of time. Finally, the human location prediction-based routing protocol (HLPRP) for mobile crowdsensing-based urban sensor networks is designed based on a HLP-based relay selection and social strengths between nodes. More specifically, the proposed routing algorithm has two phases. When a packet is generated, the proposed forwarding algorithm quickly spreads a limited number of copies of the packet throughout the network in the first phase. Then, optimal relay nodes are selected to forward the packet based on packet delivery predictability and social strength in the second phase. The details of HLPRP are presented in Chapter 5.

1.5 Thesis Organization

The rest of this dissertation is organized as follows. First, Chapter 2 discusses related works. Then, Chapter 3 describes SRMM in more detail. Chapter 4 discusses TSIRP in more detail. The detailed description of HLPRP is presented in Chapter 5. Finally, in Chapter 6, we conclude this work by summarizing our contributions and discussing future work.

Chapter 2

Related Works

2.1 Human Mobility Model

2.1.1 Real Mobility Traces

Real human movements are mostly recorded from opportunistic contacts between people using wireless devices in small areas, such as offices, conferences, and campuses. In recent years, several real traces have been collected [29–34]. Rhee et al. [29] used Garmin GPS 60CSx handheld receivers to collect human movements from five different sites (i.e., campuses of North Carolina State University, Korea Advanced Institute of Science and Technology, New York City, Disney World, and the North Carolina state fair). McNett and Voelker, [30] used 300 wireless handheld PDAs running Windows CE to record WiFi access point information over 11 weeks. Scott et al. [31] released a dataset that included five trace sets of Bluetooth sightings by groups of people carrying iMote devices. In Sensible DTU [32], $1,000$ smartphones were distributed to participants who volunteered for the study. Custom software is installed on each smartphone to record useful data (e.g., location, Bluetooth scans, WiFi scans). Olgu et al [33] collected the locations of 39 employees in an IT call center at Chicago from March 23rd, 2007 to April 17, 2007. In [34], the data of 35 students (15 students participate and they detected also 20 external devices) are gathered for 7 days on the campus of the University of Calabria.

However, the collection of human movements in real life is infeasible on a very large scale and is not flexible enough for configuring a network. It also takes a lot of resources, such as time, money, and human effort. These reasons have resulted in a limited number of available real traces. As a result, numerous synthetic models were studied to overcome the limitations. To make movements that are similar to how people move in real life, the model

needs to take into account things like pause times, flights, the radius of gyration, and ICTs and link them to the social relationships of people.

2.1.2 Synthetic Mobility Models

In early works, most mobility models were based on pure random generation of movements [1,2]. In the Markovian waypoint mobility model [1], people randomly selected destinations and pause times. The random direction model [2] randomly chooses directions of human movements. Most parameters are based on random generation without consideration of social relationships and human movement characteristics. Therefore, such models lack the regular patterns shown in daily human walks.

There are several mobility models based on human movement characteristics [5,6,35–39]. For instance, in SWIM [38], the human movement characteristics are considered and the truncated power-law distribution of ICTs is produced. In SLAW [5], spots are generated in the area and grouped into places. Then, each person selects a list of places and picks several spots in these places to visit. Selection of destinations is based on distance from the person to those spots. A spot with at a shorter distance has a higher probability of being selected. SLAW produced truncated power-law distributions of flights, ICTs, and pause times. In SMOOTH [35], them park mobility model [36] , and urban context aware mobility model [37], they also considered truncated power-law distributions of flights, ICTs, and pause times, whereas in the working day movement model [6], contact time and ICT distributions closely followed the ones found in traces from real-world measurement experiments. Royer et al. [39] analyzed national household travel survey data [40] to generate streets, avenues, and addresses in the simulation area. At the beginning of the trip, each person has an agenda that covers all day-long activities for the person. Each item on the agenda indicates when, where, and what activity the person is going to participate in. However, these models lacked consideration for the social context in human movement. Therefore, they could not completely approximate realistic human movements.

Inspired by social context, several mobility models were studied [7, 8, 41–43]. At first, studies were based on simple contexts, as done in CMM [7] and HCMM [8]. In CMM, the simulation area is divided into a number of sub-areas, and people are grouped into communities by using social relationship information. Then, each community is randomly associated with a sub-area. The attractiveness of each sub-area is determined by the current number of people in that area. HCMM retains the social model in CMM and improves on

it by adding a new concept: the home cell of each person. Specifically, the attractiveness of the home cell to home cell owners is maintained. In CMM and HCMM, selection of destinations is only affected by social relationships, which lack many regular patterns of human movements in real life (e.g., people are attracted by popular places and prefer visiting nearby places). In the sociological orbit aware location approximation and routing mobility model (ORBIT) [41], places are randomly generated in the given area, and then each person is assigned to a subset of places. A person moves around the assigned places and selects the next destination at random. As a result, the visited places for different people are not correlated, and visited places for people in real life are not considered to reproduced. Therefore, realistic human movement patterns cannot be presented.

In order to more accurately approximate the social context, in the sociological interaction mobility for population simulation model [42], a person's decision to move to a place is separated into two modes. The socialize mode is the movement toward acquaintances, and the isolate mode is intended for an escape from undesired situations. In particular, if the number of individuals in a person's current location is within a preset comfort range, the person will feel comfortable in this place and will be in socialize mode. By contrast, if the number of individuals in that place exceeds the comfort range, the person will be in isolate mode. Yang et al. [43] proposed a mobility model in which a person can belong to overlapping communities and a difference of communities in each time period. Then, each community is randomly associated with a set of places, and people randomly select destinations to visit from associated places. Those models do well in capturing the social characteristics of people. Unfortunately, they still have limitations due to a lack of consideration for human movement characteristics.

Our human mobility model addresses the limitations in the existing models. It reproduce characteristics of human movement (i.e., the distributions of flights, ICTs, radii of gyrations, and pause times all follow power-law distributions), and reflect the social context of human movement.

2.2 Routing Protocol

2.2.1 Flooding-based Routing Protocols

The flooding technique was used in a number of routing protocols [16, 17]. Under those routing protocols, messages are spread throughout the network as widely as possible. There

is a high DC because nodes continually replicate messages for newly found contacts that have not yet processed a copy of the messages. To reduce DC, several studies [18,44,45] restricted the number of times a message was replicated. However, a method to quickly spread copies of packets throughout the networks was not considered in those protocols. Moreover, those other routing protocols did not take into account the importance of selecting optimal relay nodes. As a result, messages could be forwarded to nodes that rarely interact with the destination. That results in a low PDR and high latency. To overcome this issue in our routing protocols, a method to quickly spread replications throughout the network and the selection optimal relay nodes are considered.

2.2.2 Position-based Routing Protocols

Several studies have been proposed based on the physical positions of nodes [46–49]. Specifically, the physical distances between nodes are used to select a node for forwarding. A node with a shorter distance to the destination is preferred as a relay node. However, the distances between nodes do not much affect the probability that a node will encounter the destination in the future. Therefore, the possibility of delivering messages to the destination is low. Unlike those studies, TSIRP analyzes the social interactions between nodes to estimate the probability that a node will encounter the destination in the future, whereas HLPRP uses a human location prediction model based on a RNN to estimate whether a node will meet or not meet the destination in the future.

2.2.3 Social-based Routing Protocols

A number of routing protocols have been inspired by social interaction between nodes [21, 50–55]. For instance, in [50], nodes are divided into communities, and packets were only forwarded to nodes belonging to the destination's community. In the BUBBLE Rap routing protocol [51], network communities were determined by K-clique algorithm. The local ranking of a node refers to the node's betweenness centrality in its community, whereas the global ranking refers to the node's betweenness centrality with all other nodes in the network. A message is routed to nodes that have a higher ranking. Until a node in the destination's community is found, global ranking is used. After that, local ranking is used. Under the social energy–based routing (SEBAR) routing protocol [52], a social metric based on node encounters (called social energy) is presented. A node that frequently encounters other nodes has higher social energy. The forwarding strategy is similar to the bubble rap

routing protocol [51]. The social energy of a node in the network and the social energy of a node in its community are used as the global ranking and the local ranking, respectively. In [21], a community-based opportunistic routing protocol (CORP) is proposed. The network communities are determined and a communication probability value between two communities is defined. A community has a high community probability with another community if nodes in the community frequently meet nodes in the other community. Then, if the source and the destination are in the same community, a node with high delivery predictability and high energy is selected as a relay; otherwise, nodes in the destination's community and nodes in the communities, which have higher community probabilities with the destination community, are selected. However, forming communities is challenging in those routing protocols since a node must have all the information on all other nodes. In [53–55], relay selection was based on centrality metrics. Specifically, packets were routed to nodes with a greater centrality value. Nevertheless, forwarding a large number of messages to central nodes results in congested traffic and long delays around those nodes. To resolve those issues, TSIRP focuses on social interactions between nodes with the destination and HLPRP focuses on probability of meeting the destination, instead of using centrality measurements. In other words, a relay node is more specifically chosen in our proposed routing protocols. Based on that, traffic congestion and delays can be avoided.

2.2.4 Encounter History-based Routing Protocols

Based on nodes' encounter histories, a number of routing protocols were proposed [19, 20, 56–59]. In [20, 56], delivery predictability was proposed based on encounter history. This value indicates how likely a node will be able to send a message to the destination. If a node encounters another node with a higher value for delivery predictability to the destination, the node replicates the message. Under [19,57–60], delivery predictability was also used for relay selection. Furthermore, those protocols control and limit the number of replications to reduce DC. These routing protocols' metrics (e.g., delivery predictability) could represent how frequently two nodes have interacted in the recent past. However, they cannot estimate when the two nodes will encounter each other in the future. Two nodes may interact frequently in the present, but their next contact may happen in the distant future. For example, two students frequently meet each other in the morning when they attend the same class but do not meet again until the next morning. Therefore, the delivery predictability might be high at present, but the two nodes might not meet in the near future. As a result, optimal

relay nodes might not be selected, and the routing protocols are unable to achieve high performance.

In [61], the social network is detected from the history of encounters between nodes. In the detected social network (DSN), the link between two nodes exists if they encounter each other. The degree centrality of nodes is obtained on the DSN graph. Moreover, the friendship information between nodes on online social networking websites, such as Facebook, LinkedIn is used to calculate tie strength between two nodes. The tie strength between two nodes is the number of online social networks where they are friends. The interest of nodes is also collected and used to form an interest network where there is a link between two nodes if they have at least one common interest. The number of common neighbors over the total neighbor of two nodes in the interest network is considered as the link predictor between them. Based on the degree centrality, the tie strength, and the link predictor, a metric is proposed for relay selection. A node with a higher value of relay selection metric is preferred to become a relay node. In [62], the history of encounters is also used to obtain DSN graphs for each time slot of a day, in which the weight of links is the number of contacts between nodes in a time slot. In addition, they define a dynamic online social network (DOSN), in which there is a link between two nodes if they are online friends (e.g., Facebook friends) and the weight between two nodes is calculated based on common interest and the number of encounters between them in a time slot. Two nodes with a lot of common interest and a larger number of encounters have a stronger weight. From the DSN graph and DOSN graph, weighted degree centralities are obtained for nodes. Based on those weighted degree centralities, the temporal fused degree centrality is proposed. A node with high values of weighted degree centralities has a high value of the temporal fused degree centrality. The forwarding strategy is based on the bubble rap routing protocol [51] with the temporal fused degree centrality, which is used as the ranking of nodes. Under those protocols, to determine network communities, a node needs to know information about all the other nodes in the network. That is difficult. The friendship information on online social networking websites and the interest of nodes are helpful information for routing. However, in a large network size such as urban sensor networks, it is also hard to require a node to know the interest of all other nodes and share their personal information with other nodes. Moreover, when the centrality measurements such as degree centrality are used for relay selection, central nodes are preferred to be selected as relay nodes. It may be effective when the network traffic is low. However, for the high network traffic, forwarding a lot of messages to central nodes

leads to long delays and congested traffic around those nodes.

Chapter 3

Social Relationship-Aware Human Mobility Model

3.1 Preliminaries

In this section, the terms used in the human mobility model are presented. First, Kullback-Leibler (KL) divergence [63], Kolmogorov-Smirnov (K-S) test [64], and weighted mean relative difference (WMRD) [65], which measure the similarity between two distributions, is described. Then, the model selection criteria (i.e., the Akaike information criterion [66] and the Bayesian information criterion [66]) are considered.

3.1.1 Kullback–Leibler Divergence

In order to measure how a probability distribution diverges from another distribution, Kullback et al. [63] introduced KL divergence. This value can show the directed divergence and can measure the distance between two probability distributions. A lower value for KL divergence indicates that two distributions are more similar. Let P and Q be two probability distributions. The KL divergence of Q from P is denoted as $D_{KL}(P||Q)$.

For discrete probability distributions $P(i)$ and $Q(i)$, $D_{KL}(P||Q)$ is defined as follows [67]:

$$D_{KL}(P||Q) = \sum_i P(i)\log\frac{P(i)}{Q(i)} \tag{3.1}$$

In practice, it may incur a log of zero. To avoid this, all probabilities have a small positive constant added.

3.1.2 Kolmogorov-Smirnov Test

Two-sample K-S test [64] is used to measure the similarity between two distributions of two data samples. Let $\boldsymbol{X}$ and $\boldsymbol{Y}$ be the two given data samples. The cumulative distribution function of $\boldsymbol{X}$ and $\boldsymbol{Y}$ are denoted as $F_x(i)$ and $F_y(i)$, respectively. H denotes the K-S statistic. H is defined as:

$$H = max_i |F_x(i) - F_y(i)| \tag{3.2}$$

h_0 is a null hypothesis that data sample $\boldsymbol{X}$ and data sample $\boldsymbol{Y}$ come from the same distribution. μ defines a significance level. For a given μ value, a critical value can be obtained from a table in [64]. Let H_μ be the critical value for level μ. If $H \leq H_\mu$, h_0 is accepted at significance level μ. The maximum value of significance level μ, which still satisfies the condition $H \leq H_\mu$, is defined as P value. In other words, if $\mu \leq P$, h_0 is accepted. P value can show the possibility that two samples come from the same distribution. A higher P value means that distributions of two data samples are more similar.

3.1.3 Weighted Mean Relative Difference

Weighted mean relative difference (WMRD) [65] is used to compare the difference between two probability distributions. Let P and Q be two probability distributions. WMRD between P and Q is defined as follow:

$$WMRD = \frac{\sum_i |P(i) - Q(i)|}{\sum_i \frac{P(i) + Q(i)}{2}} \tag{3.3}$$

WMRD value presents the difference between two probability distributions. A higher WMRD value means that two probability distributions are more different. In other words, two probability distributions are more similar if WMRD between them is low.

3.1.4 Model Selection Criteria

We assume that there are a given dataset and a set of models. Then, model selection criteria can be used to find the best model to match the given dataset. In this paper, we use the Akaike information criterion (AIC) and the Bayesian information criterion (BIC).

To calculate AIC and BIC, maximum likelihood estimation (MLE) [68] is used first to find an estimator that maximizes the likehood function [68]. Let $\boldsymbol{D}$ be the given data set. A model has probability distribution f by unknown parameter $\boldsymbol{\lambda}$, which could be a vector.

$L(\boldsymbol{\lambda}|\boldsymbol{D})$ denotes the likehood function of the model with data $\boldsymbol{D}$. $L(\boldsymbol{\lambda}|\boldsymbol{D})$ is defined as:

$$L(\boldsymbol{\lambda}|\boldsymbol{D}) = \prod_{i \in \boldsymbol{D}} f(i|\boldsymbol{\lambda}) \tag{3.4}$$

MLE finds an estimator $\hat{\boldsymbol{\lambda}}$ that maximizes the likelihood function.

- *AIC* is the model selection criterion established by a relationship between KL divergence and MLE. The quality of the models is estimated by AIC values. A lower AIC value indicates that the model is a better fit to the given data. Let us define the number of estimated parameters to be $n_{\boldsymbol{\lambda}}$. The AIC is calculated as:

$$AIC = -2\log(L(\hat{\boldsymbol{\lambda}}|\boldsymbol{D})) + 2n_{\boldsymbol{\lambda}} \tag{3.5}$$

- *BIC* is another model selection criterion based on information theory but set within Bayesian context. The model with the lowest BIC is preferred. Let $n_{\boldsymbol{D}}$ be the number of data samples in $\boldsymbol{D}$. BIC is defined as:

$$BIC = -2\log(L(\hat{\boldsymbol{\lambda}}|\boldsymbol{D})) + n_{\boldsymbol{\lambda}}\log(n_{\boldsymbol{D}}) \tag{3.6}$$

3.2 The Proposed Human Mobility Model

In this section, the model for SRMM is presented. Then, SRMM is described in four phases. In phase 1, people are partitioned into social groups by using information from a social graph. In phase 2, we describe how spots are generated and grouped into places. The candidate places and the candidate spots are selected in phase 3. Finally, in phase 4, the destination spots for people are determined.

3.2.1 Model

In our problem, human movements are reproduced in a considered area. In this area, we assume there is a set of places, $\mathbb{S}_P = \{P_i | 1 \leqslant i \leqslant n_P\}$, where n_P is the number of places. Each place, P_i, consists of multiple spots. Let the set of spots in the considered area be $\mathbb{S}_s = \{s_i | 1 \leqslant i \leqslant n_s\}$, where n_s is the number of spots. In other words, place P_i is an area (e.g., mall, park, or hotel) that includes a set of spots. A spot, s_i, is a staying point on the map, such as a clothing store in a mall, or a bench in a park.

Among all people, social relationships exist that affect human movements. We partition people into social groups that represent realistic communities, such as groups of friends, families, and football teams. Each group includes people, who have close relationships. In the considered area, we denote the set of people as $\mathbb{S}_u = \{u_i | 1 \leqslant i \leqslant n_u\}$ and the set of social groups as $\mathbb{S}_G = \{G_i | 1 \leqslant i \leqslant n_G\}$, where n_u and n_G are the number of people and the number of groups, respectively. Several regular patterns are usually present in human movements. For example, people tend to visit their friends and visit popular places where there are many spots. Each individual prefers to visit certain places, rather than other places.

Table 3.1: Definitions of sets.

Notation	**Meaning**
$\mathbb{S}_P = \{P_i \| 1 \leqslant i \leqslant n_P\}$	The set of places
$\mathbb{S}_s = \{s_i \| 1 \leqslant i \leqslant n_s\}$	The set of spots
$\mathbb{S}_u = \{u_i \| 1 \leqslant i \leqslant n_u\}$	The set of people
$\mathbb{S}_G = \{G_i \| 1 \leqslant i \leqslant n_G\}$	The set of social groups
$\mathbb{S}^u_{FP}$	The set of frequently visited places for person u
$\mathbb{S}^u_{FS}$	The set of frequently visited spots for person u
$\mathbb{S}^u_{RP}$	The set of randomly visited places for person u
$\mathbb{S}^u_{RS}$	The set of randomly visited spots for person u
$\mathbb{S}^u_{CP} = \mathbb{S}^u_{FP} \cup \mathbb{S}^u_{RP}$	The set of candidate places for person u
$\mathbb{S}^u_{CS} = \mathbb{S}^u_{FS} \cup \mathbb{S}^u_{RS}$	The set of candidate spots for person u

3.2.2 Phase 1: Human Grouping

In this phase, a clustering algorithm is utilized to detect social groups in a social graph, which is provided as input.

The social graph illustrates the strengths of closeness among people. The strength of social closeness between two people is assumed to be in the range [0,1]. Figure 3-1 shows an example of a social graph with 10 people $(u_1, u_2, ..., u_{10})$. The strength between u_1 and u_2

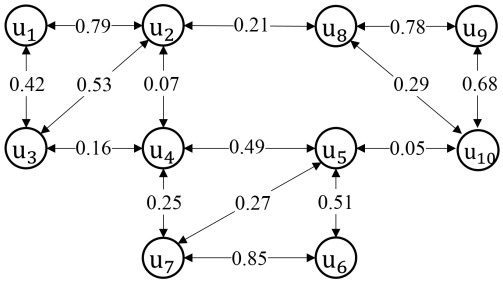

Figure 3-1: The social graph

equals 0.79, whereas the strength between u_5 and u_{10} equals 0.05. There is no connection link between u_5 and u_8. This implies that the strength is 0. The social graph can also be presented as a matrix where the entries are the closeness strengths among the people.

For detection of social groups in the input social graph, we use a spectral clustering algorithm [69]. The spectral clustering algorithm is simple to implement in practice and usually outperforms traditional algorithms such as the K-means algorithm [70]. Recall that n_G is the number of social groups, and n_u is the number of people. By using the spectral clustering algorithm, people who have strong relationships will be grouped in a social group. From n_u people, n_G social groups are generated. Specifically, the spectral clustering algorithm utilizes the social matrix and n_G as the inputs. Based on the social matrix, a Laplacian matrix is constructed by using a symmetric normalized technique [71]. After that, we calculate the set of eigenvectors for the Laplacian matrix. Then, people are represented in a lower-dimensional space, $\mathbb{R}^{n_u \times n_G}$, which is formed by the first n_G eigenvectors that correspond to the n_G lowest eigenvalues. At the final step of the spectral clustering algorithm, the K-means algorithm is used on this data space to obtain social group set $\mathbb{S}_G = \{G_i | 1 \leqslant i \leqslant n_G\}$. Each social group G_i includes a set of people.

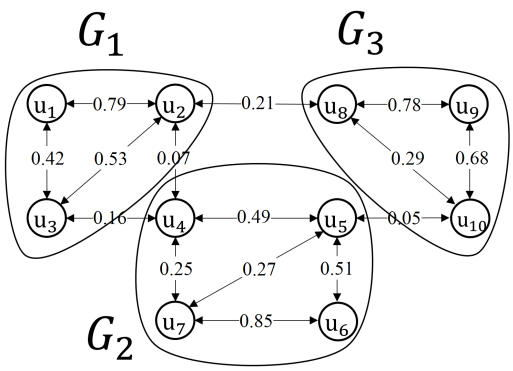

Figure 3-2: The social groups

An example of the clustering result is shown in Figure 3-2. We obtain social group set

$\mathbb{S}_G = \{G_1, G_2, G_3\}$ from the social graph, where G_1 includes u_1, u_2, u_3; G_2 includes u_4, u_5, u_6, u_7; and G_3 includes u_8, u_9, u_{10}.

3.2.3 Phase 2: Generation of Spots

In this phase, spots in $\mathbb{S}_s$ are generated in the area and then grouped into places. Lee et al. [72] reported that visited spots of human in real life can be reproduced as fractal spots. This means that people always tend to gather in popular places, which conforms to contexts in real life, such as homes, parks, schools, and workplaces. In order to generate fractal spots, SRMM utilizes the bursty spot model (BSM) [72]. From real trace data [29], the real-spot distribution for New York City is shown in Figure 3-3(a), and an example of a synthetic map obtained by using BSM is displayed in Figure 3-3(b). As shown in the figures, the dispersion of spots on the synthetic map is similar to the real map.

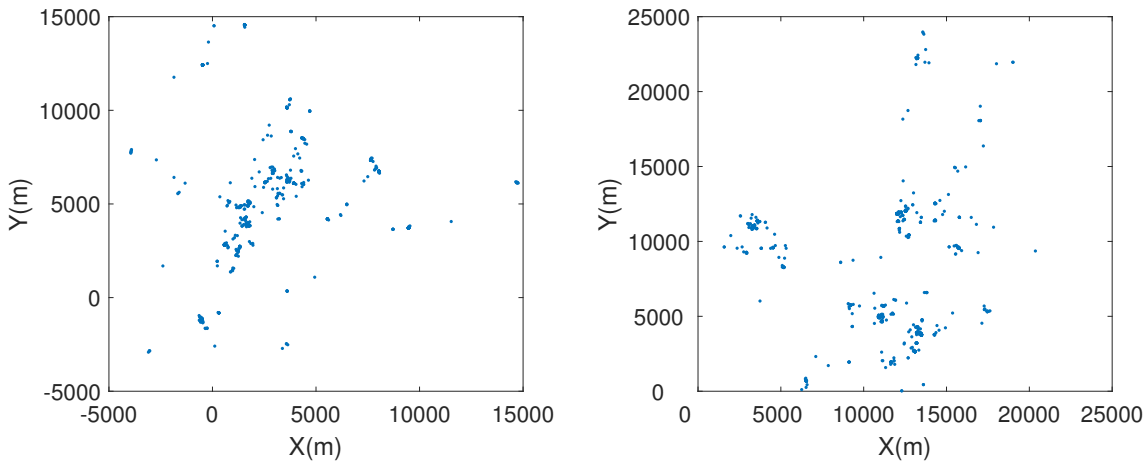

(a) New York City real map.

(b) The synthetic map generated by BSM.

Figure 3-3: The dispersions of spots on the map.

After generating a synthetic map with fractal spots, the set of places, $\mathbb{S}_P = \{P_i | 1 \leqslant i \leqslant n_P\}$, is formed by grouping spots in circles with radius r in meters. For example, in order to form place P_i, a spot is selected as the center of place P_i. To select the center spot, spots are considered one by one in increasing order of X-coordinates of spots. In the case that X-coordinates of spots are equal, spots in increasing order of Y-coordinates of spots are considered. If a spot does not belong to any places, it will be selected as the center spot of place P_i. Then, spots, which are within a radius of r meters from the center spot and do not belong to any places, will be grouped into place P_i. In this way, place P_i includes a set

of spots within a range of r meters. The selection of r value is based on the transmission range of wireless personal area networks.

3.2.4 Phase 3: Selection of Candidate Places and Candidate Spots

In this phase, each social group is associated with a set of places. The associated places are called frequently visited places. Then, each person in the same social group selects a set of spots from their frequently visited places to obtain their frequently visited spots. Let G be a social group in $\mathbb{S}_G$ and u be a person in G. The set of frequently visited places and the set of frequently visited spots for person u are denoted as $\mathbb{S}^u_{FP}$ and $\mathbb{S}^u_{FS}$, respectively.

In addition, at the beginning of each day trip, each person newly selects another place as a randomly visited place, then picks several spots in this place as randomly visited spots. Let $\mathbb{S}^u_{RP} = \{RP^u\}$ be the set of randomly visited places for person u, where RP^u is the randomly visited place of person u. The set of randomly visited spots of person u is denoted $\mathbb{S}^u_{RS}$.

On a day trip, $\mathbb{S}^u_{CP} = \mathbb{S}^u_{FP} \cup \mathbb{S}^u_{RP}$ is the set of candidate places for person u, and $\mathbb{S}^u_{CS} = \mathbb{S}^u_{FS} \cup \mathbb{S}^u_{RS}$ is the set of candidate spots for person u.

The operation of this phase is presented in three steps as follows:

- *Step 1: Selecting frequently visited places*

  People in a social group often visit the same places. That is a common context in real life. For example, a group of friends usually visits the same mall, park, and restaurant. In SRMM, each social group is associated with several places called frequently visited places. Accordingly, people in the same social group have the same frequently visited places. We define random variable x as the number of frequently visited places selected for a social group. Let A be a place in $\mathbb{S}_P$, and n^A_s denotes the number of spots in place A. Let $P_{G,A}$ be the probability that social group G selects place A as a frequently visited place. $P_{G,A}$ is calculated as:

$$P_{G,A} = \frac{(n^A_s)^\theta}{\sum_{i \in \mathbb{S}_P} (n^i_s)^\theta} \tag{3.7}$$

  where θ ($\theta > 0$) is a parameter that adjusts the effect of the number of spots in selecting frequently visited places. Eq. (3.7) indicates that a place with more spots has a higher probability of being selected. That agrees with the context in real life whereby most people prefer visiting popular places with more popularly visited points, rather than

unpopular places. A higher θ also implies that several places with more spots will be frequently selected by social groups. In contrast, a lower θ value will reduce the possibility that different social groups will select the same frequently visited places.

- *Step 2: Selecting frequently visited spots*

  We define random variable y ($0 \leq$y$\leq 100\%$) as a percentage value. After obtaining the set of frequently visited places ($\mathbb{S}^u_{FP}$), person u randomly picks y percent of the spots from each place in $\mathbb{S}^u_{FP}$ as frequently visited spots (where person u usually visits during day trips).

- *Step 3: Selecting a randomly visited place and randomly visited spots on a day trip*

  In order to match the context of real life (on a day trip, a person visits not only frequently visited spots but additional spots, on occasion), this step randomly selects a new place and new spots at the beginning of each day.

  First, social group G randomly selects a number of new places. The number of new places is denoted as z. Then, person u randomly chooses a place from the z newly selected places as the randomly visited place (RP^u), and picks y percent of the spots in RP^u to obtain randomly visited spots.

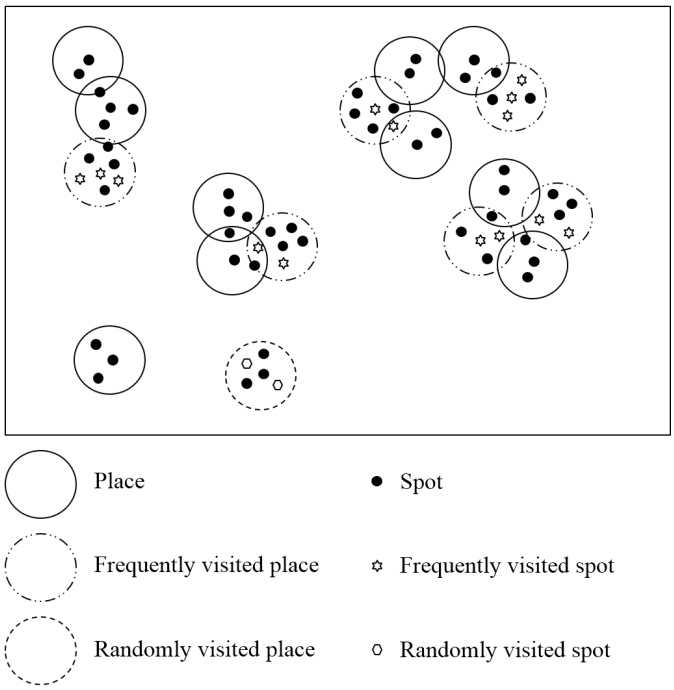

Figure 3-4: Candidate places and candidate spots for person u.

The values of random variables x, y, and z in this phase are assumed to follow truncated

normalized distributions. The distributions of these random variables can be adjusted to reflect various situations in real life. For example, people living in an urban area have more visited places and visited spots than people living in a mountain area.

Now, the candidate places and the candidate spots are obtained. An example of chosen places and spots for person u is shown in Figure 3-4.

3.2.5 Phase 4: Selection of the Destination Spots

In this step, person u first randomly chooses a spot in S^u_{FS} as the home spot. Each day person u starts the trip from this spot. The home spot for person u is denoted as h^u. Then, from $\mathbb{S}^u_{CP}$ obtained in phase 3, person u selects a place to visit. Let SP^u denote the selected place. Finally, person u selects a destination spot from the candidate spots in place SP^u.

Now, the process for selecting the destination spot of person u is presented in detail. This process comprises two steps.

- *Step 1: Person u selects place SP^u from set $\mathbb{S}^u_{CP}$ to visit*

  Based on the assumption that people usually prefer visiting nearby places rather than faraway places, and they are also attracted to places where many of their friends are visiting, SRMM considers two components (the distances from the places to person u's current location, and the social relationships of person u) while selecting place SP^u from set $\mathbb{S}^u_{CP}$.

  Let i be an arbitrary place in $\mathbb{S}^u_{CP}$. In order to obtain the probability that person u visits place i, two probability components are used.

  First, we consider the probability related to distance. Let $d_{u,i}$ denote the distance from person u to place i. $P^D_{u,i}$ denotes the probability of selection related to distance. This probability is calculated as:

$$P^D_{u,i} = \frac{\left(\dfrac{1}{d_{u,i} + c_d}\right)^{\alpha}}{\sum_{j \in \mathbb{S}^u_{CP}} \left(\dfrac{1}{d_{u,j} + c_d}\right)^{\alpha}} \tag{3.8}$$

  where an adjustment parameter, α ($\alpha > 0$), modifies the effect of the distance. In order to avoid situations where the distance from person u to a place is 0, we use a small constant, $c_d > 0$. Eq. (3.8) implies that a place within a shorter distance has a higher value for $P^D_{u,i}$.

Secondly, we consider the probability of selection related to social relationships. Recall that person u belongs to group G. Let $n_u^{G,i}$ be the number of people, who are currently visiting place i and belong to group G. We define $P_{u,i}^S$ as the probability of selection related to social relationships. $P_{u,i}^S$ is calculated as:

$$P_{u,i}^S = \frac{(n_u^{G,i} + c_s)^\beta}{\sum_{j \in \mathbb{S}_{CP}^u} (n_u^{G,j} + c_s)^\beta} \tag{3.9}$$

where parameter β ($\beta > 0$) adjusts the effect of social relationships, and a small constant, $c_s > 0$, is used to avoid a result where $n_u^{G,i} = 0$. Eq. (3.9) indicates that a place with many friends of person u has a higher value for $P_{u,i}^S$.

Finally, we define $P_{u,i}^{DS}$ as the probability that person u chooses to visit place i. $P_{u,i}^{DS}$ is calculated by combining two components, $P_{u,i}^D$ and $P_{u,i}^S$, as follows:

$$P_{u,i}^{DS} = \rho \times P_{u,i}^D + (1 - \rho) \times P_{u,i}^S \tag{3.10}$$

where a tunable parameter, $\rho \in [0, 1]$, modifies the balance between distance and social relationship.

- *Step 2: Person u selects a destination spot in SP^u*

  Let $\mathbb{C}_{SP}^u$ denote the set of candidate spots that are in place SP^u for person u. In this step, person u selects a spot in $\mathbb{C}_{SP}^u$ as the destination spot. Let s be a spot in $\mathbb{C}_{SP}^u$, and let $l_{u,s}$ be the distance from person u to spot s. $P_{u,s}$ denotes the probability that person u selects spot s as the destination spot. This probability is calculated as:

$$P_{u,s} = \frac{\left(\frac{1}{l_{u,s}}\right)^\gamma}{\sum_{j \in \mathbb{C}_{SP}^u} \left(\frac{1}{l_{u,j}}\right)^\gamma} \tag{3.11}$$

  where adjustment parameter γ ($\gamma > 0$) is used to adjust the effect of the distance. Eq. (3.11) indicates that spots near person u have higher probability values, which also agrees with the real-life context.

In SRMM, everyday person u is assumed to move from 7:00 to 19:00 (i.e., 12 hours per day). On a day trip, person u starts moving from home spot h^u and comes back to home spot h^u at t_c, i.e., t_c is the homecoming time of person u. The value of t_c is assumed to

follow a truncated normalized distribution.

3.3 Evaluation Results and Discussion

In this work, Matlab was used to validate the proposed social relationship−aware human mobility model. We take into account human movement characteristics and social relationships of the mobility model. First, KL divergence, K-S test, WMRD are used to show how well the human movement characteristics generated by the mobility model match a real trace. Then, to validate the fitting of the human movement characteristics with truncated power-law distributions, AIC and BIC values are used. Finally, a new performance metric (the same social group ratio) is used to evaluate the reflection of social relationships. The results obtained with SRMM are compared with the results from SLAW [5], CMM [7], and ORBIT [41].

3.3.1 Simulation Setup

Let T denote simulation time. As many as movements of 100 people for $T = 200$ h are generated. According to results shown in [73], the movement speed of people is set to follow a truncated normalized distribution $N(4.6, 1^2)$ km/h. The communicating nodes' transmission range is set to 100 m, which is the typical transmission range for Bluetooth Low Energy. For grouping spots into places, the radius r is also set to 100 m. In this work, it is assumed that two people encounter each other when they are within transmission range for 30 s.

For x, y, and z, we use $N(7, 2^2)$, $N(20, 5^2)$, and $N(3, 1^2)$, respectively. Homecoming time t_c is set to follow $N(18, 0.5^2)$. This means that the time to come back to home spot of people is randomly chosen from 17:30 to 18:30. To obtain social graphs in real life, a list of survey questions (e.g., where people usually come? where are the favorite places? and what are the favorite activities of people?) needs to be collected and analyzed to evaluate social strengths between people. In this work, we simply model social matrix $M_{n_u,p}$ in which n_u is the number of people in the area, p is the probability that two people have a social connection, and the strengths of the social links follow a uniform distribution within a range of values from 0 to 1. In this simulation, we use social matrix $M_{100,0.2}$. The sojourn distribution used in SRMM follows a truncated power-law distribution with a range of values from 0.5 to 700 min.

In addition, SLAW, CMM, and ORBIT models are also examined to compare them with our model. Common parameters, such as the area of simulation, the transmission range, the number of people, and the simulation time, use the same values in all models. In SLAW, the value of the constant a in least-action trip planning [5] is set to 1.5 (the best value shown in SLAW). The number of hubs in the ORBIT model follows the number of places in our model. In CMM, the simulation area is presented by as a grid; we set the size of each square on the grid to $100m \times 100m$, and we set the number of social groups to the same value as our model. Otherwise, we use the input parameters described in their studies. Details of the simulation parameters can be found in Table 3.2.

Table 3.2: Simulation parameters.

Parameter	**Value**
Radius of places (r)	100 m
Number of people (n_u)	100
Simulation time (T)	200 h
Speed of people	$N(4.6, 1^2)$ km/h
Transmission range	100 m
Social matrix	$M_{100,0.2}$
Number of social groups (n_G)	10
Number of frequently visited places (x)	$N(7, 2^2)$
Percentage value of spots picked from candidate places (y)	$N(20, 5^2)$
Number of new places selected by a group at the beginning of each day (z)	$N(3, 1^2)$
Homecoming time (t_c)	$N(18, 0.5^2)$

3.3.2 Synthetic Map

In this section, the simulation area is established to approximate the measurement sites of the New York City trace from Rhee et al. [29]. The area's size is $24km \times 24km$, and the number of spots, n_s, is $1,120$. The parameters for generating spots with the BSM are calculated in the same way used by Lee et al. [5].

3.3.2.1 Verifying the Human Movement Characteristics

In SRMM, the pause-time distribution was already set to follow a truncated power-law distribution with a range of values from 0.5 to 700 min. Thus, this section verifies other human movement characteristics (i.e., the distributions of flights, the radii of gyration, and ICTs). First, KL divergence, K-S test, WMRD are used to validate our model with the real trace. Several studies analyzed real traces, and showed that the distributions of flights, radii of gyration, and ICTs in real traces follow truncated power-law distributions [3,4,9]. Therefore, AIC and BIC between a truncated power-law distribution and an exponential distribution over human characteristics are compared to show whether the human characteristics follow truncated power-law distributions or not.

3.3.2.1.1 Flight

We first consider the flight distribution with various parameter values for SRMM. Figure 3-5 shows KL divergence between the real trace flight distribution and the synthetic ones generated by SRMM using various parameter values. A lower value for KL divergence implies that generated flight lengths are a better fit to the real trace.

In Figure 3-5a, KL divergence with various values for α is presented. In general, KL divergence decreases when α increases from 0.8 to 1.6, and increases when α increases from 1.6 to 2.0. The values for KL divergence show that SRMM matches the real flight distribution well, especially when α is equal to 1.6.

Figure 3-5b shows the effect of β on KL divergence. Overall, the flight distributions are close to the real flight, and when $\beta = 1.6$, the flight distribution is a better fit to the real flights than the others.

KL divergence with various values of ρ is shown in Figure 3-5c. In general, KL divergence values decrease when ρ increases from 0.4 to 0.8. When $\rho = 0.8$, the flight distribution is the closest approximation to the real one. When $\rho = 1$ (i.e., the social relationships between people are not considered), the KL divergence value is larger than KL divergence in case $\rho = 0.8$. This indicates that to obtain flights that match the real flights well, the social relationship is important, and it should be considered.

Figure 3-5d displays the KL divergence values with various values of γ. As shown in the figure, we obtain the best result for KL divergence when $\gamma = 0.8$.

In Figure 3-5e, KL divergence with various values of θ is presented. As shown in the

results from KL divergence, all synthetic flights fit closely to the real one. when $\theta = 0.8$, the flight distribution is a better fit to the real flights than the others.

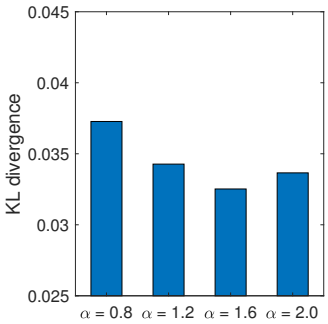

(a) Various α values ($\beta = 1.6, \rho = 0.8, \gamma = 0.8, \theta = 0.8$).

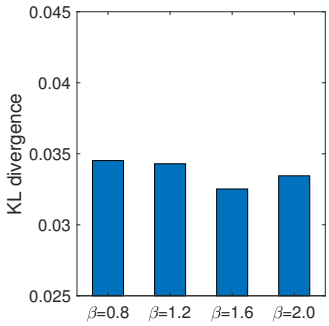

(b) Various β values ($\alpha = 1.6, \rho = 0.8, \gamma = 0.8, \theta = 0.8$).

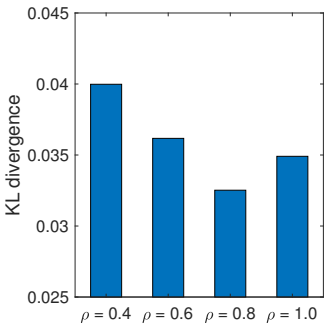

(c) Various ρ values ($\alpha = 1.6, \beta = 1.6, \gamma = 0.8, \theta = 0.8$).

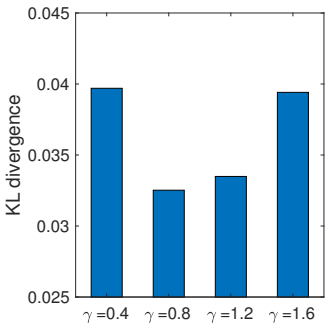

(d) Various γ values ($\alpha = 1.6, \beta = 1.6, \rho = 0.8, \gamma = 0.8, \theta = 0.8$).

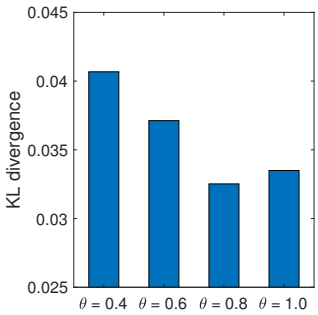

(e) Various θ values ($\alpha = 1.6, \beta = 1.6, \rho = 0.8, \gamma = 0.8$).

Figure 3-5: KL divergence between the real trace flight distribution and the synthetic ones generated by SRMM using various values for the parameters.

Following results of KL divergence in Figure 3-5, the values of $\alpha, \beta, \rho, \gamma$, and θ in SRMM are set to $1.6, 1.6, 0.8, 0.8$, and 0.8, respectively.

Now, we verify our flight distribution with results from other models. The flight distributions obtained from various models are shown in Figure 3-6a, and the closeness of the flight distributions in synthetic models to real flights is shown by values in Table 3.3. A model with a lower value for KL divergence and WMRD, and a higher value for P value of K-S test implies that the model is a better fit to the real trace. From the figure and the values shown in Table 3.3, it is clear that SRMM most closely matches the real flight distribution. For example, KL divergence with SRMM is 0.0325, whereas SLAW and CMM are 0.0625 and 0.3205, respectively. SRMM also obtained the lowest value for WMRD (i.e., 0.7716)

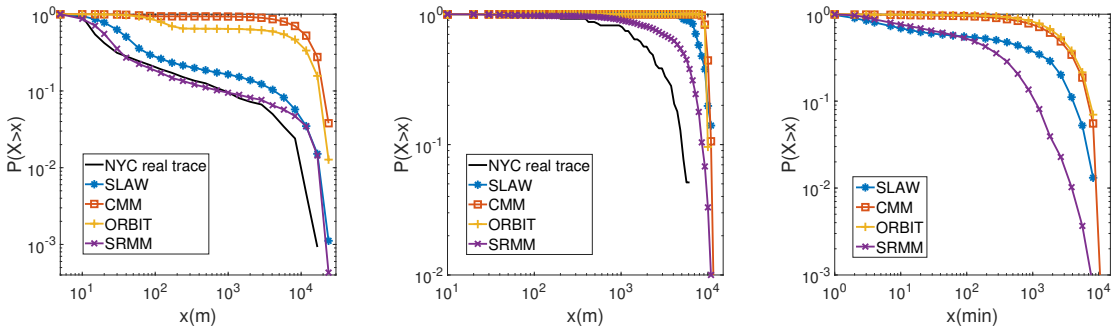

(a) Flight distributions.

(b) The radius of gyration distributions.

(c) ICT distributions.

Figure 3-6: Human movement characteristics for various models with the synthetic map

and the highest value of P value of K-S test (i.e., 1.01×10^{-24}). The flight distribution with SLAW is also close to the real trace. In ORBIT and CMM, the spots were not generated by using fractal spots, and the distance was not considered when choosing the destinations. These are the main reasons for a large difference between these models and the real trace.

Table 3.3: KL divergence, P value of K-S test, and WMRD between the real trace distributions and the distributions generated by the synthetic models.

	SRMM		**SLAW**		**CMM**		**ORBIT**	
	Flight	**Radius of Gyration**	**Flight**	**Radius of Gyration**	**Flight**	**Radius of Gyration**	**Flight**	**Radius of Gyration**
KL divergence	0.0325	0.5211	0.0625	0.6627	0.3205	0.6921	0.2985	0.7223
WMRD	0.7716	1.9260	0.9868	1.9900	1.8420	2.0000	1.6658	2.0000
P value of K-S test	1.01×10^{-24}	0.5180	8.88×10^{-119}	4.63×10^{-16}	0	2.23×10^{-24}	0	3.02×10^{-26}

To check whether the generated flight distributions follow truncated power-law distributions, Table 3.4 shows AIC and BIC results between a truncated power-law distribution and an exponential distribution. As shown in Table 3.4, the flight distribution generated by SRMM is closer to a truncated power-law distribution than to an exponential distribution. The results also indicate that flight distributions generated by other models approximate truncated power-law distributions.

Table 3.4: Results from AIC and BIC of the New York City trace (NYC) and various synthetic models with the synthetic map (the truncated power-law distribution (Pow), the exponential distribution (Exp), the radius of gyration (RoG)).

	SRMM			**SLAW**			**CMM**			**ORBIT**			**NYC**		
	Flight	**RoG**	**ICT**	**Flight**	**RoG**	**ICT**	**Flight**	**RoG**	**ICT**	**Flight**	**RoG**	**ICT**	**Flight**	**RoG**	**ICT**
Selected model by AIC	Pow	Pow	Pow	Pow	Pow	Pow	Pow	Pow	Pow	Pow	Pow	Exp	Pow	Pow	N/A
Selected model by BIC	Pow	Pow	Pow	Pow	Pow	Pow	Pow	Pow	Pow	Pow	Pow	Exp	Pow	Pow	N/A

3.3.2.1.2 The radius of gyration

To validate the real radius of gyration, Figure 3-6b shows the radius of gyration distributions for the various models, and Table 3.3 presents the KL divergence between the real radius of gyration distribution and distributions generated by the synthetic models. As shown in Figure 3-6b and Table 3.3, the radius of gyration distribution generated by SRMM is closest to the distribution extracted from the real trace. Specifically, the radius of gyration generated by SRMM obtains the lowest values for KL divergence (i.e., 0.5211) and WMRD (i.e., 1.9260), and the highest value of P value of K-S test (i.e., 0.5180).

Table 3.4 presents the results of AIC and BIC between a truncated power-law distribution and an exponential distribution over the radius of gyration of the New York City trace and various synthetic models. AIC and BIC results indicate that the radius of gyration produced by SRMM is closer to a truncated power-law distribution than an exponential distribution.

3.3.2.1.3 Inter-contact time

There is no available contact information in the real trace [29,30]; hence, only ICT distributions from synthetic models are shown in Figure 3-6c. The ICT distribution generated by SRMM is close to the ICT distribution of SLAW.

To validate the truncated power-law distribution, the distributions in Figure 3-6c are also verified with AIC and BIC. The results from AIC and BIC are provided in Table 3.4. As can be seen in the table, ICT distributions generated by SRMM, SLAW, and CMM fit better to power-law distributions, whereas the ICTs of ORBIT fit better to an exponential distribution. The ICTs of CMM are usually a very long time since people can move to any of the places without periodicity, so the chances of two people meeting again after the first encounter are much lower. In ORBIT, each person randomly chooses a list of places and

then randomly picks a place in that list to visit. Thus, two people rarely encounter each other, and the ICTs of ORBIT are also very long times.

3.3.2.2 Verifying Social Relationships

In this section, we evaluate how well the mobility models reflect social relationships. First, we define the same social group ratio (SSGR), and we describe how to calculate this value. Then, the obtained results for the same social group ratio are presented.

3.3.2.2.1 The same social group ratio

Mobility models and corresponding output mobility traces should reflect social relationships embedded in the input social graph. Please note that from a mobility trace of a mobility model, a social graph can also be obtained based on encounter rates between people (i.e., people, who have high encounter rates, will have strong relationships). A mobility model well reflects social relationships in the input social graph if the social graph obtained from the mobility trace of the model is similar to the input social graph. To determine the similarity between those two social graphs, social groups, which are obtained from those social graphs, are compared. People in a social group have strong social relationships. Therefore, if social groups in two social graphs are similar, two social graphs should be similar. To compare social groups in two social graphs, a new performance metric, called the same social group ratio (SSGR), is defined. Specifically, a set of social groups, $\mathbb{S}_G$, is obtained by using information from the input social graph. Based on the mobility trace generated by the mobility model, we also obtain a social graph and another set of social groups. Let this set be $\mathbb{S}_G^{syn}$. Then, for each group in $\mathbb{S}_G$, we select a corresponding group from $\mathbb{S}_G^{syn}$ to form a pair of groups. Please note that each group is only assigned to one pair, and pairs of groups are determined to maximize the number of common people in those pairs. The ratio of the total number of common people in all pairs to the total number of people in the network is defined as the same social group ratio. A high value for SSGR indicates that the mobility model highly reflects the social relationship. For example, $\mathbb{S}_G = \{G_1, G_2, G_3\}$. Group G_1 consists of u_1, u_2, and u_3; u_4 and u_5 belong to group G_2; group G_3 includes u_6 and u_7. For $\mathbb{S}_G^{syn} = \{G'_1, G'_2, G'_3\}$; u_1, u_2, and u_4 belong to group G'_1; group G'_2 includes u_3 and u_5; group G'_3 consists of u_6 and u_7. Based on maximizing the common people in pairs of groups, groups (G_1, G_2, G_3) in $\mathbb{S}_G$ correspond to groups (G'_1, G'_2, G'_3) in $\mathbb{S}_G^{syn}$, respectively. Specifically, the pair (G_1, G'_1) has two common members, u_1 and u_2. The pair (G_2, G'_2) has

one common member, u_5, while u_6 and u_7 are two common members in the pair (G_3, G'_3). The total for the common members is 5. We obtain SSGR = 0.83.

To calculate SSGR values for synthetic models, we performed the following process.

- First, we find the social group set, $\mathbb{S}_G$. Set $\mathbb{S}_G$ is extracted from the social matrix during phase 1 in SRMM. For a fair comparison in SRMM, SLAW, CMM, and ORBIT, the same social group set is used.

- Secondly, to determine set $\mathbb{S}_G^{syn}$, we analyze the synthetic trace of each model to obtain a matrix of encounter rates (ER). The values in the ER matrix are the number of times people encounter each other over the total simulation time. Suppose m and n denote two arbitrary people. $E_{m,n}$ denotes the number of encounters between m and n during simulation time T. Let $b_{ER}(m,n)$ be the encounter rate between m and n. Then, $b_{ER}(m,n)$ is calculated as:

$$b_{ER}(m,n) = \frac{E_{m,n}}{T} \tag{3.12}$$

  In reality, people who have strong relationships tend to meet each other frequently [74, 75]. Thus, a higher value in the ER matrix can represent a stronger relationship between people. Then, the ER matrix is used by the spectral clustering algorithm to obtain social group set $\mathbb{S}_G^{syn}$. The values in the ER matrix are normalized to within the range [0,1] before the matrix is used in spectral clustering.

- Finally, we compare $\mathbb{S}_G$ and $\mathbb{S}_G^{syn}$ to obtain the SSGR value.

3.3.2.2.2 The results of the same social group ratio

SSGR values from various models are shown in Figure 3-7. As can be seen in the figure, the results obtained from CMM and SRMM are higher than from SLAW and ORBIT because only CMM and SRMM consider social relationships between people. SRMM takes into account many social contexts, whereas CMM considers only a few, which leads to the higher SSGR with SRMM. Specifically, in CMM model, the destination can be selected from all places in the network. There are no set of frequently visited places for the people in a social group and no set of candidate places as in our model. Therefore, people in a social group have a low possibility to encounter in a wide area. That leads to a lower value of SSGR.

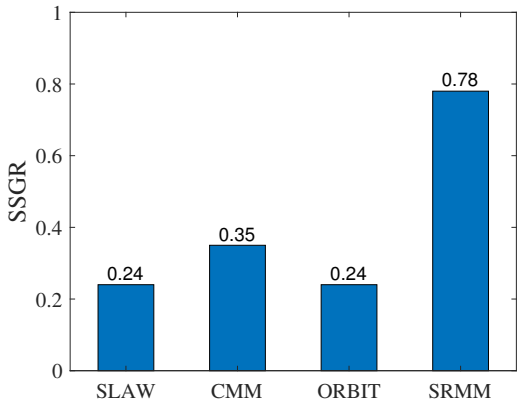

Figure 3-7: The same social group ratio values from various models with the synthetic map.

Because the number of social groups (n_G) in the area is not considered in SLAW and ORBIT, that does not affect human movements in that models. Therefore, Figure 3-8 only displays SSGR with different n_G values in CMM and SRMM. In general, SSGR values decrease when n_G increases. People in CMM may visit different places in the network, so increasing n_G leads to a significant decrease in the probability that people will visit the places their social friends are visiting. Therefore, when n_G is a higher value, SSGR from CMM is lower and close to the SSGR values from ORBIT and SLAW. In contrast, in SRMM, people in the same social group have the same frequently visited places and usually encounter each other. Thus, we still obtain a high value of SSGR from SRMM.

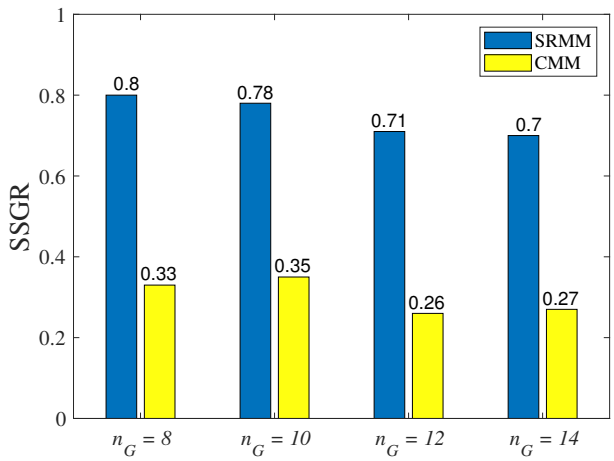

Figure 3-8: The same social group ratio values for SRMM and CMM from various n_G values.

3.3.3 Real Road Map

In this section, to obtain more realistic human movements, the mobility models are considered on the real road map. For generating spots on the map, the bursty spot model is also used. First, spots are normally generated, and then spots are mapped to the nearest point on the nearest road on the map.

In this simulation, we use the real road map of Helsinki downtown [76]. The size of this map is 8.3 km × 7.31 km and the number of generated spots, n_s, is set to 978. Figure 3-9 shows generated spots on the real road map of Helsinki downtown.

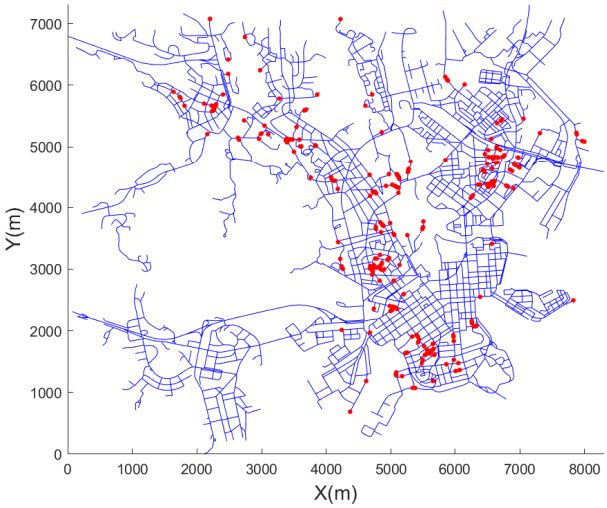

Figure 3-9: Generated spots on the real road map of Helsinki downtown.

In the mobility models, to move between two spots on the real road map, the shortest path between two spots is used. This path is obtained by using Dijkstra's algorithm [77].

3.3.3.1 Verifying the Human Movement Characteristics

In this section, the distributions of flights, ICTs, and the radius of gyration are presented. AIC and BIC criteria are also used to verify that flights, inter-contact time, and the radius of gyration follow truncated power-law distributions. There are no available real mobility traces on the real road map of Helsinki downtown. Therefore, the KL divergence for comparing the synthetic models with real traces is not collected.

3.3.3.1.1 Flight

To validate the flight distribution, Figure 3-10a presents flight distributions from various models on the real road map. As can be seen in the figure, most of the flights from CMM and ORBIT are long flights. Flights generated by SRMM and SLAW are similar and more natural than the flights from CMM and ORBIT. Table 3.5 shows AIC and BIC results between a truncated power-law distribution and an exponential distribution. From the figure and the values shown in Table 3.5, it is clear that the flight distributions from SRMM, SLAW, and CMM fit better to power-law distributions, whereas the flights of ORBIT fits better to an exponential distribution.

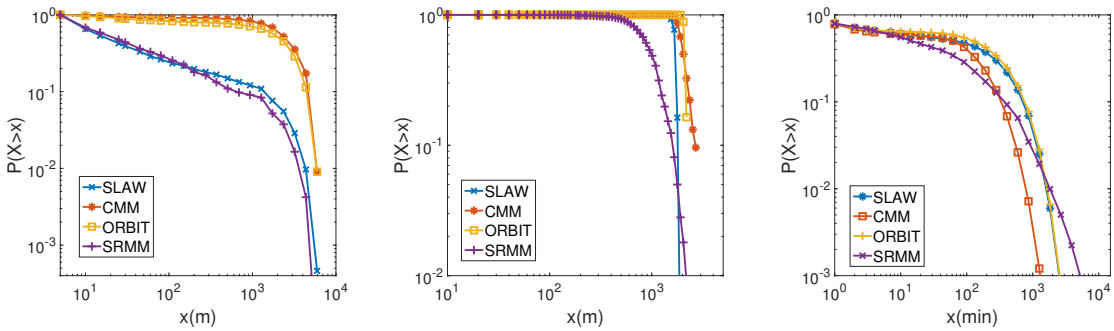

(a) Flight distributions. (b) The radius of gyration distributions. (c) ICT distributions.

Figure 3-10: Human movement characteristics for various models with the real road map

Table 3.5: Results from AIC and BIC of various synthetic models with the real road map of Helsinki downtown.

	SRMM			**SLAW**			**CMM**			**ORBIT**		
	Flight	**RoG**	**ICT**	**Flight**	**RoG**	**ICT**	**Flight**	**RoG**	**ICT**	**Flight**	**RoG**	**ICT**
Selected model by AIC	Pow	Pow	Pow	Pow	Pow	Pow	Pow	Pow	Pow	Exp	Pow	Pow
Selected model by BIC	Pow	Pow	Pow	Pow	Pow	Pow	Pow	Pow	Pow	Exp	Pow	Pow

3.3.3.1.2 The radius of gyration

To check whether the generated radius of gyration distributions follow a truncated power-law distribution, the radius of gyration distributions from various models are shown in Figure 3-10b and Table 3.5 presents the results of AIC and BIC between a truncated power-

law distribution and an exponential distribution over the radius of gyration. As shown in Figure 3-10b, the radius of gyration from SRMM is lower than those from other models. AIC and BIC results indicate that the radius of gyration generated by SRMM and all other models are closer to truncated power-law distributions than exponential distributions.

3.3.3.1.3 Inter-contact time

Figure 3-10c shows the ICT distributions from various mobility models. As shown in the figure, ICTs generated by SRMM are shorter than ICTs from other models since in our model, people in the same social group tend to frequently meet. Please note that the results of AIC and BIC are provided in Table 3.5. AIC and BIC results indicate that ICT distributions generated by SRMM, SLAW, CMM, and ORBIT fit better to power-law distributions than exponential distributions.

3.3.3.2 Verifying Social Relationships

In this subsection, the same social group ratio is obtained to verify that the mobility model can embody social relationships. Figure 3-11 presents SSGR values from various models. As can be seen in the figure, SSGR from CMM is slightly higher than from SLAW and ORBIT. The best result of SSGR is obtained from SRMM (i.e., 0.78), which indicates that social contexts between people are well embedded into our mobility model.

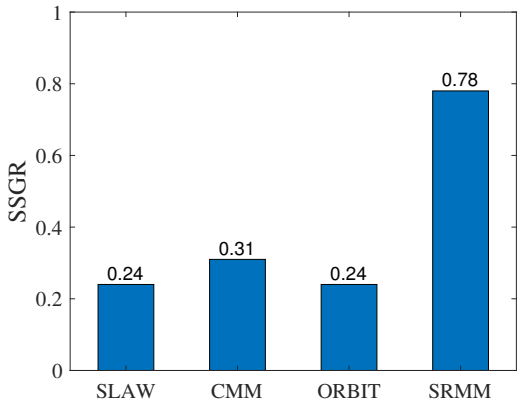

Figure 3-11: The same social group ratio values from various models with the real road map.

3.4 Chapter Summary

In this Chapter, we proposed a novel human mobility model to address the limitations of existing human mobility models. The human mobility model is important for validating

the network performance of routing protocols in OMSNs. Our proposed model takes into account the characteristics of human movement and the social context in human movement. Specifically, SRMM captures flights, the radius of gyration, ICTs, and pause times for realistic human movement. Then, many real contexts are considered in our model. For example, people prefer visiting nearby locations and are attracted to popular places. In the same social group, people usually tend to visit each other, and have the same frequently visited places. By reproducing real contexts, SRMM reflects social relationships in human movement. To validate human movement characteristics, SRMM is considered on the synthetic map and the real road map. The results were compared with real human movements in a New York City trace and in other models (SLAW, CMM, and ORBIT). At first, KL divergence was used to show how well models match real traces. Then, AIC and BIC were used to evaluate the fit with truncated power-law distributions of human movement characteristics. Finally, we defined the same social group ratio to validate the reflection of social relationships in human mobility models. The experiment results indicate that human movements from SRMM are more closely approximate real human movement characteristics, and clearly reflect the social relationships among people when we compare with other models.

Chapter 4

Temporal Social Interactions-Based Routing Protocol

4.1 The Network Model and Problem Definition

In this section, first, the network model is present. Then, the problem definition is discussed.

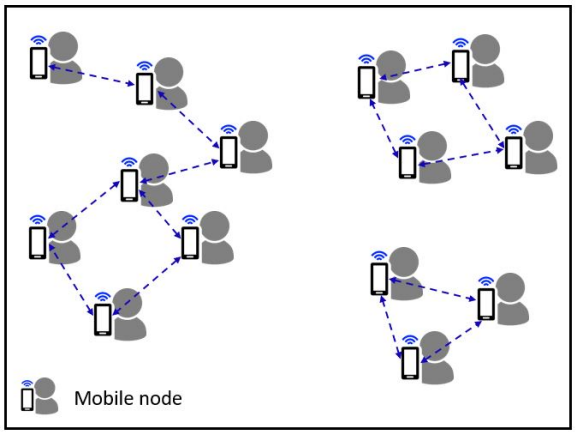

Figure 4-1: The network model.

Figure 4-1 shows the network model. A city-wide network is considered. Specifically, N nodes move in a city area. Those nodes communicate and exchange messages with each other via wireless interfaces (e.g., Bluetooth 5.0) when they come within the communication range of each other without infrastructures. Messages in this network can be of different data types, such as text, images, and video. This network model can achieve the quick and low-cost deployment, which is suitable for emergency situations such as natural disaster and military conflicts.

This work addresses the problem of how to effectively route messages between mobile nodes. Selection of relay nodes is an important issue. The movement history of nodes is collected over D days. In the movement history, the positions of the nodes are recorded. Each day is divided into time slots. Two nodes are considered as encountering each other when they are within transmission range for 30 seconds. Let denote the movement history information as M. Each packet includes three attributes: source, destination, time to live (TTL). TTL is a time value in seconds that limits the lifetime of the packet in the network. After TTL expires, the packet is dropped. Our work considers the network performance in terms of DC, PDL, and PDR. DC is calculated by dividing the total number of replications by the total number of messages generated. PDL is the time it takes for messages to be delivered from sources to destinations. PDR measures the number of messages delivered to their intended destinations divided by the total number of messages. Node u wants to send a message to edge node v. Let $\mathbb{S}_u^{NB}$ denote the set of neighboring nodes of node u. The objective is to choose relay nodes in $\mathbb{S}_u^{NB}$ to maximize PDR and minimize PDL and DC, given M with the constrain TTL.

4.2 TSIRP routing protocol

In this section, we first describe the potential forwarding metrics, and how to calculate them. Then, the spreading rate control value is discussed. Finally, the TSIRP forwarding scheme is described.

4.2.1 Potential Forwarding Metric

In this work, movement history is analyzed to obtain potential forwarding metrics (PFMs), which are used for relay selection. A node with a lower PFM value is preferred as a relay node. Based on the inter-contact time, the expected delivery delay, and the meeting probability condition, three PFMs are proposed.

4.2.1.1 The mean value of inter-contact time ($\overline{ICT}$)

The inter-contact time (ICT) represents the elapsed time between two successive contacts for a given pair of nodes. Let u and v denote two arbitrary nodes in the network. The mean value of ICTs between node u and node v is denoted $\overline{ICT}_{u,v}$. Let η be the number of ICT samples between node u and node v obtained from the movement history. For example,

suppose that in the movement history, node u and node v encounter three times. We will obtain two ICT samples (i.e. $\eta = 2$). The elapsed time between the first encounter and the second encounter is the first sample of ICT. The elapsed time between the second encounter and the third encounter is the second sample of ICT. The ith ICT sample is denoted $ICT^{i}_{u,v}$. $\overline{ICT}_{u,v}$ is calculated as follows:

$$\overline{ICT}_{u,v} = \frac{\sum_{i=1}^{\eta} ICT^{i}_{u,v}}{\eta} \tag{4.1}$$

A low value of $\overline{ICT}_{u,v}$ means that node u frequently meets node v. Therefore, the node that has the lower mean value for inter-contact time with the destination is preferred as a relay node. $\overline{ICT}_{u,v}$ is used as a potential forwarding metric.

4.2.1.2 The expected delivery delay (ED)

Note that the movement history of nodes is collected over D days, and one day in the movement history is divided into 36 time slots. To determine whether two nodes encounter each other or not in a time slot, the encounter state is used. Let $e^{u,v}_{d,i}$ denote the encounter state between node u and node v in time slot i of day d, such that $e^{u,v}_{d,i}$ equals 1 if node u encounters node v in time slot i of day d; otherwise, $e^{u,v}_{d,i}$ is zero.

We define $P^{u,v}_{i}$ as the probability that node u meets node v in time slot i of a new day. Based on the social interactions between two people at a certain time, $P^{u,v}_{i}$ is estimated as follows:

$$P^{u,v}_{i} = \frac{1}{D} \sum_{d=1}^{D} e^{u,v}_{d,i} \tag{4.2}$$

Equation (4.2) indicates that if node u has frequently encountered node v in time slot i in the past, $P^{u,v}_{i}$ will have a large value (i.e., node u has a high possibility to encounter node v in time slot i in the future).

In time slot, t, the expected delivery delay between node u and node v within k time slots is denoted as $ED^{u,v}_{t}$. $ED^{u,v}_{t}$ is the estimated latency to deliver packets from node u to node v. In other words, $ED^{u,v}_{t}$ is the expected duration from the time slot t to the time when node u encounters node v. This value is obtained as follows:

$$ED^{u,v}_{t} = \sum_{i=t+1}^{t+k} ((i-t) \times P^{u,v}_{i} \times \prod_{j=t+1}^{i-1} (1 - P^{u,v}_{j})) \tag{4.3}$$

where $(i-t)$ is PDL if node u and node v encounter at time slot i. $P_i^{u,v}$ is the estimated probability that node u encounters node v at time slot i. $\prod_{j=t+1}^{i-1}(1-P_j^{u,v})$ is the estimated probability that node u and node v have not encountered (and hence have not delivered packets) before time slot i. Based on those two probabilities, the probability that node u delivers a packet to node v in time slot i, and has not delivered the packet to node v in previous time slots (i.e., time slot $t+1$ to time slot $i-1$) is calculated, and then $ED_t^{u,v}$ is obtained. The expected delivery delay within k time slots of the two nodes is used as a potential forwarding metric. A node with a lower expected delivery delay to the destination is the better forwarder

4.2.1.3 The number of time slots to satisfy the meeting probability condition ($\hat{x}$)

In current time slot, t, $P^{u,v}(x)$ denotes the probability that node u meets node v during x time slots, $P^{u,v}(x)$ is calculated as:

$$P^{u,v}(x) = 1 - \prod_{i=t}^{t+x}(1 - P_i^{u,v}) \tag{4.4}$$

Given a required meeting probability, ϑ, we find the minimum value of x that satisfies the condition $P^{u,v}(x) \geq \vartheta$. Let $\hat{x}$ be the minimum value of x that satisfies the meeting probability condition:

$$\hat{x} = \{\min(x) | P^{u,v}(x) \geq \vartheta\} \tag{4.5}$$

$\hat{x}$ is used as a potential forwarding metric. A lower value for $\hat{x}$ means the required meeting probability between the two nodes can be obtained in a shorter time. Thus, a node is selected as the relay node if it has a lower value of $\hat{x}$ with the destination.

4.2.2 Spreading Rate Control Value

In this subsection, the forwarding token for packets is discussed first. Then, we propose a spreading rate control value to control the message spreading rate.

In TSIRP, the number of replications is limited by using a forwarding token. When a node generates a packet, it also assigns a forwarding token for the packet in a similar way to spray-and-wait [18]. The initial value of the forwarding token is C. When a node replicates a packet, it also appends half of the current token value to the copy of the packet. When

the token value is less than or equal to 1, the node stops spreading the packet and waits until meeting the destination.

Now, we describe the proposed spreading rate control value based on the forwarding token value and the residual lifetime of a packet. Suppose that node u wants to send packet p to node v. The current forwarding token value for packet p at node u is denoted c_p^u. When node u tries to replicate packet p to its neighbor, c_u^p is checked. If $c_u^p \leq 1$, node u stops spreading the packet and waits until meeting the destination; otherwise, relay selection is performed and the spreading rate control value is used.

Let t_p be the residual lifetime of packet p. The spreading rate control value for packet p of node u is denoted as SC_p^u. SC_p^u is calculated as follows:

$$SC_p^u(c_u^p, t_p) = e^{-[\chi \times \frac{c_u^p}{C} + (1-\chi) \times (\frac{t_p}{TTL})]} \tag{4.6}$$

where a tunable parameter, $\chi \in [0, 1]$, modifies the balance between the residual lifetime and the forwarding token. From Equation (4.6), we see that $SC_p^u \in [1/e, 1)$ and higher values of t_p and c_p^u lead to a lower value for SC_p^u.

The spreading rate control value is used in the forwarding scheme to control the message spreading rate. Specifically, a low value of SC_p^u means that packet p has just been generated (i.e., the residual lifetime of the packet is long), and the token value for forwarding it is large. Therefore, packet p should quickly spread through the network. When the packet is spread wide enough (i.e., SC_p^u is large), the rate for spreading the packet should be reduced to decrease DC.

Let κ ($\kappa \in [1/e, 1]$) denote the threshold value for the spreading rate control. When $1/e \leq SC_p^u \leq \kappa$, node u replicates packet p to all neighbor nodes without considering any metrics. That increases the rate for spreading packet p. If $SC_p^u > \kappa$, relay nodes are selected and node u only replicates packet p to those relay nodes, which reduces the rate for spreading packet p.

4.2.3 Forwarding Algorithm

The proposed forwarding scheme based on PFMs and the spreading rate control value is presented in Algorithm 1. The notations in the algorithm are defined in Table 4.1.

Suppose that a person (node u) wants to share a photo (packet p) with a friend (node v) by interfacing with an application. The routing for the message is processed in the network

Algorithm 1 The forwarding scheme

Node u wants to send packet p to node v
Input: $\mathbb{S}_u^{NB} = \{n_i | 1 \leq i \leq n_u^{NB}\}, SC_p^u, \kappa, PFM_{u,v}, \overline{C_D(u)}, t_p, d_t, c_u^p$
Initialize $i = 1$;
while $i \leq n_u^{NB}$ and $c_u^p > 1$ **do**
    if $\frac{1}{e} \leq SC_p^u \leq \kappa$ **then**
        Node n_i is selected as a relay node for packet p
    else if $PFM_{n_i,v} < PFM_{u,v}$ **then**
        Node n_i is selected as a relay node for packet p
    else if $TTL - t_p > d_t$ and $\overline{C_D(n_i)} > \overline{C_D(u)}$ **then**
        Node n_i is selected as a relay node for packet p
    end if
    if node n_i is selected as a relay node for packet p **then**
        Node u forwards a copy of packet p to node n_i
        $c_{n_i}^p = \frac{c_u^p}{2}$
        $c_u^p = \frac{c_u^p}{2}$
    end if
    $i = i + 1$
end while

Table 4.1: Definitions of notations in the forwarding scheme

Notation	Meaning
n_u^{NB}	The number of neighbors of node u
$\mathbb{S}_u^{NB} = \{n_i \| 1 \leq i \leq n_u^{NB}\}$	The neighbor set of node u after sorting in increasing order of values for PFMs between the neighbor nodes and the destination
SC_p^u	The spreading rate control value for packet p of node u
$\kappa \in [1/e, 1]$	The threshold value for the spreading rate control
$PFM_{u,v}$	The potential forwarding metric between node u and node v
$\overline{C_D(u)}$	The mean value of degree centrality for node u
t_p	The residual lifetime of packet p
d_t	The time threshold for determining a long-delayed packet
c_u^p	The forwarding token for packet p of node u

layer. Specifically, the neighbor list of node u is checked. If the destination is in its neighbor list, the packet is delivered to the destination. If not, the forwarding scheme is executed.

As described in Table 4.1, the neighbors of node u are sorted in increasing order of PFM values between the neighbor nodes and the destination. Recall that a node with a lower PFM value is considered better for relaying packet p. Therefore, packet p should be forwarded to the node with a lower PFM value. For this, relay selection is performed with each neighbor n_i, where i is from 1 to n_u^{NB}.

For each node n_i, the packet forwarding token of node u, c_u^p, is checked in line 3. If $c_u^p \leq 1$, node u stops forwarding and waits until meeting the destination; otherwise, relay selection begins and the spreading rate control value (SC_p^u) is checked in line 4. If SC_p^u is a low value (i.e., $1/e \leq SC_p^u \leq \kappa$), in line 5, node u selects node n_i as the relay node for packet p without considering any other metrics. With a high SC_p^u value (i.e., $SC_p^u > \kappa$), the relay node is selected based on PFMs.

PFM values are compared in line 6. In particular, if node n_i has a lower PFM with the destination than node u (i.e., $PFM_{n_i,v} < PFM_{u,v}$), node n_i is selected as the relay node for packet p in line 7.

In our forwarding scheme, if a packet cannot be delivered to the destination for a long time, degree centrality is also used to create more chances to deliver the packet to the destination. Specifically, the residual lifetime of packet p is taken into account in line 8. $TTL - t_p > d_t$ indicates that packet p is experiencing a long delay. For such packets, degree centrality, which is the number of links to a node, is used. Degree centralities of nodes are obtained for each day in the movement history, and then, the mean value of degree centrality is calculated. A node with a higher mean value for degree centrality shows that it has many neighbors and more chances to meet better relay nodes. Therefore, if $\overline{C_D(n_i)} > \overline{C_D(u)}$, node u will select node n_i as the relay node for packet p.

Finally, if node n_i is selected as the relay node for packet p, in lines 12-14, node u will forward a copy of packet p to node n_i, and a half of the forwarding token value is assigned to the copy of packet p at node n_i.

4.3 The Analytical Model

In the analytical model, it is assumed that N nodes are in the network, each with a finite transmission range, and moving in a closed area. Two nodes encounter when they come within the transmission range of each other, at which point they can exchange packets. It

is assumed that each node has enough buffer to store all packets that it has received. A packet has the time to live (TTL) and it is dropped if TTL expires.

To design a feasible mathematical model, yet obtain an analytical insight into the proposed routing protocol, the behavior of TSIRP is slightly simplified. Specifically, the meeting probability is used instead of using PFMs and the degree centrality in case of long delay packets is not considered. For example, node u wants to send packet p to node v. Let n_i be a neighbor of node u. After checking the forwarding token value (i.e, $c_u^p > 1$) and the spreading rate control value (i.e., $SC_p^u > \kappa$), if node n_i has a higher meeting probability with the destination than node u, it will be selected as the relay node for packet p.

In order to obtain the analytical model, first, the network state is discussed. Then, the state transition is described. Finally, an absorbing Markov chain is used to obtain the network performance. The meaning of notations, which are used in the analytical model, are shown in Table 4.2.

4.3.1 Network Sate Space

Let us focus on a single packet p from source node u to destination v. A bit is used to represent the state that a node carries the packet or not. If the node carries the packet, the state bit is set to 1; otherwise, the state bit is set to 0. Let $S = \{0, 1\}$ be the node state space. For N nodes in the network, the space of network state is a set of N - element vectors, possibly restricted by a number of constraints. Let $\Omega \subseteq S^N$ denote the network state space.

$$\Omega = \{X|X = (x_1, x_2, x_3, ..., x_N)\}, \qquad x_i \in S \tag{4.7}$$

where x_i represent the state of node i in the network.

The number of replications is limited by forwarding token value C. Therefore, the network state space has a constraint as follow:

$$\sum_{i=1(i \neq v)}^{N} x_i \leq C \tag{4.8}$$

4.3.2 State Transition

We assume that the network is in a state during a time slot, and the network state transition is considered when the time slot changes. Specifically, the state transition happens if the packet is forwarded to new nodes in the next time slot. An example of state transitions for

Table 4.2: Important notation in the analytical model

Notation	Meaning
$S = \{0, 1\}$	The node state space
Ω	The network state space
p_i^C	The probability that $c_i^p > 1$
$p_t^R(i, j)$	The probability that node j receives packet p from node i at time slot t
Ω_X	The set of potential next states with current state X
$\mathbb{R}_X$	The set of relay nodes in state X
$p_t^R(j)$	The probability that node j receives packet p at time slot t
$p(X, Y)_t$	The probability that the network state switches from X to Y at time slot t
$\mathbb{S}^{TR}$	The set of transient states
n^{TR}	The number of transient states
$\mathbb{S}^{AB}$	The set of absorbing states
n^{AB}	The number of absorbing states
$\mathbf{Q}_i^t$	The transition matrix between transient states at time slot t with $t_p = TTL - i$
$\mathbb{Q}^t$	The set of all transition matrix $\mathbf{Q}_i^t$ at time slot t
$\mathbf{R}_i^t$	The transition matrix from transient states to absorbing states at time slot t with $t_p = TTL - i$
$\mathbb{R}^t$	The set of all transition matrix $\mathbf{R}_i^t$ at time slot t
$\mathbf{N}^t$	The fundamental matrix for packets, which is generated at time slot t
$\mathbf{B}^t$	The absorbing probabilities matrix for packets, which are generated at time slot t
$p_t^I(Z)$	The probability that the initial network state is state Z
$p_d(X^*)$	The probability that the final network state is absorbing state X^*
p_d	The packet delivery ratio
δ_{i,X^*}^t	The expected number of steps until absorbing state X^*, when starting at state i
τ	The duration of a time slot
ED	The delivery delay

six nodes in the network with the initial forwarding token $C = 4$ is shown in Fig. 4-2. The network state switches from state X_1 to state X_2 when node 2 forwards the packet to node 5, and from state X_2 to X_3 when the packet is forwarded to node 4. In TSIRP, the state transition from X_3 to state X_1 is impossible.

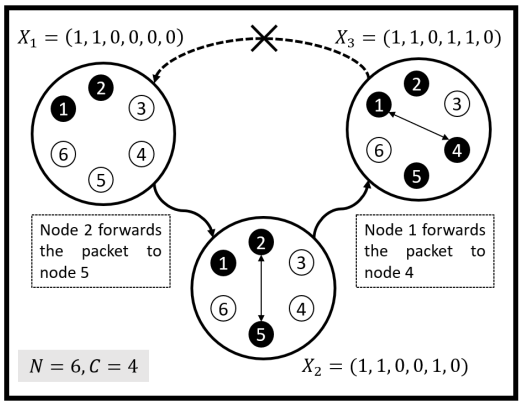

Figure 4-2: Example of state transitions for six nodes with initial forwarding token $C = 4$

To study state transition, first, the probability that a relay node i forwards packet p to node j is discussed. Then, the transition between network states is presented.

Now, it is assumed that there is a contact between relay node i and node j. In the case that node j is the destination, packet p is delivered to node j. Otherwise, the forwarding scheme is taken into account. Specifically, the forwarding token value is checked. Recall that c_i^p is the forwarding token for packet p of node i. For node i to transfer packet p to node j, the first condition is $c_i^p > 1$. The number of relay nodes in state X is defined as n_X^R ($n_X^R = \sum_{i=1}^{N} x_i$). Let p_i^C denote the probability that $c_i^p > 1$, which is approximated one if n_X^R is lower than $\frac{C}{2}$. Otherwise, p_i^C is approximated as:

$$p_i^C = \frac{C - n_X^R}{n_X^R} \tag{4.9}$$

In the case that $c_i^p > 1$, let $p_t^R(i, j)$ be the probability that node j receives packet p from node i at current time slot t. Then, $p_t^R(i, j)$ is obtained as follow:

$$p_t^R(i, j) = \begin{cases} P_t^{i,j}, & \text{if } j = v \\ p_i^C \times P_t^{i,j}, & \text{if } j \neq v \text{ and } (\frac{1}{e} \leq SC_p^i \leq \kappa \text{ or } P_t^{j,v} > P_t^{i,v}) \\ 0, & \text{otherwise} \end{cases} \tag{4.10}$$

where if node j is the destination (i.e., $j = v$), $p_t^R(i, j)$ is equal to the probability that node

i encounters node j at time slot t ($P_t^{i,j}$). In the case of $j \neq v$, the spreading rate control value and the meeting probability are checked. Specifically, if $\frac{1}{e} \leq SC_p^i \leq \kappa$ or $P_t^{j,v} > P_t^{i,v}$, $P_t^{i,j}$ is calculated based on p_i^C and $P_t^{i,j}$. Otherwise, the packet is not be forwarded.

Now, we consider the transition between network states. Let $X = (x_1, x_2, ..., x_n)$ and $Y = (y_1, y_2, ..., y_n)$ be two network states in Ω, and also let X be the current network state. For Y to be a potential next state from current state X, y_i should be equal to 1 if x_i is 1. Let Ω_X be the set of potential next states from current state X. We assume that $Y \in \Omega_X$. $\mathbb{S}_{X,Y}^D$ defines a set of nodes, which have the different state between X and Y. Specifically, $x_j = 0$ and $y_j = 1$, $\forall j \in \mathbb{S}_{X,Y}^D$. Every contact between a relay node i ($x_i = 1$) and node $j \in \mathbb{S}_{X,Y}^D$ offers the chance for transiting from current state X to state Y. Let $\mathbb{R}_X$ be the set of relay nodes in state X and $p_t^R(j)$ be the probability that node j receives packet p at time slot t. $p_t^R(j)$ is calculated as:

$$p_t^R(j) = 1 - \prod_{i \in \mathbb{R}_X} (1 - p_t^R(i,j)) \tag{4.11}$$

where the probability that node j has not received the packet from any nodes in $\mathbb{R}_X$ is computed. Then, the $p_t^R(j)$ could be obtained as Eq. (4.11).

If the packet is transferred to all nodes in $\mathbb{S}_{X,Y}^D$ and was not transferred to any other nodes, then the network transition from state X to state Y happens. Let $\mathbb{R}_Y$ be the set of relay nodes in state Y. The probability that the network state switches from X to Y at current time slot t is defined as $p(X,Y)_t$, which is obtained as follow:

$$p(X,Y)_t = \begin{cases} \prod_{i \in \mathbb{S}_{X,Y}^D} p_t^R(i) \times \prod_{j=1 (j \notin \mathbb{R}_Y)}^N (1 - p_t^R(j)), & \text{if } X \neq Y \\ 1 - \sum_{Z \neq X} p(X,Z)_t, & \text{if } X = Y \end{cases} \tag{4.12}$$

where if $X \neq Y$, the probability that all nodes in $\mathbb{S}_{X,Y}^D$ receive the packet and the probability that all nodes, which are not relay nodes in state Y, do not receive the packet are calculated. Then, $p(X,Y)_t$ is obtained. In the case of $X = Y$, which means that the network state is not be changed, $p(X,Y)_t$ is calculated based on the probability that the state transition does not happen.

4.3.3 Network Performance

In this subsection, the routing protocol is transformed into an absorbing Markov chain. Then, network performance metrics such as PDR and PDL in routing are obtained.

An absorbing Markov chain is a Markov chain in which every state can reach an absorbing state after some number of steps. An absorbing state is a state that, once entered, is impossible to leave. States, which are not absorbing states, in an absorbing Markov chain are defined as transient states. To transform the routing protocol into an absorbing Markov chain, a network state is considered as a state in the absorbing Markov chain. From the network state space (Ω), states, in which the destination has not received the packet, are defined as transient states, and states, in which the packet was delivered to the destination, are considered as absorbing states. When the network state is a transient state, it may switch to another transient state or an absorbing state. When the network state is an absorbing state, further transitions are no longer considered. The transition matrix between transient states and the transition matrix from transient states to absorbing states are obtained from the probability of state transitions. Based on those matrices, the fundamental matrix and the absorption probabilities matrix for the absorbing Markov chain are calculated. Then, network performance is obtained using those matrices.

Specifically, we consider the network state when transferring packet p from source node u to destination v. Any state $X \in \Omega$, with $x_v = 0$ and $x_i = \{0, 1\}, \forall i \neq v$, is considered as the transient state. The set of transient states is denoted as $\mathbb{S}^{TR}$. The desired network state is any $X^* \in \Omega$, with $x_v = 1$ and $x_i = \{0, 1\}, \forall i \neq v$. These states are absorbing states. Let $\mathbb{S}^{AB}$ be the set of absorbing states. n^{TR} and n^{AB} denote the number of transient states and the number of absorbing states, respectively.

Now, the transition matrix between transient states is considered. It is assumed that TTL of packet p is k time slots. Note that t_p is the residual lifetime of packet p, and the spreading rate control value depends on t_p. The value of t_p decreases from k to 0. For each time slot t, a set of matrices $\mathbb{Q}^t = (\mathbf{Q}_0^t, \mathbf{Q}_1^t, ..., \mathbf{Q}_{k-1}^t)$ is obtained. Where $\mathbf{Q}_i^t$ is the transition matrix between transient states at time slot t, with $t_p = TTL - i$. An element $q_{n,m}^t$ in matrix $\mathbf{Q}_i^t$ represents the probability that a state transits from transient state n to transient state m at time slot t. The size of matrix $\mathbf{Q}_i^t$ is $n^{TR} \times n^{TR}$.

For the transition matrix from transient states to absorbing states, another set of matrices $\mathbb{R}^t = (\mathbf{R}_0^t, \mathbf{R}_1^t, ..., \mathbf{R}_{k-1}^t)$ is also obtained. $\mathbf{R}_i^t$ is a $n^{TR} \times n^{AB}$ matrix, which is the transition matrix from transient states to absorbing states at time slot t with $t_p = TTL - i$. Each element $r_{n,m}^t$ in matrix $\mathbf{R}_i^t$ shows the probability that state switches from transient state n to absorbing state m at time slot t.

Now, the fundamental matrix for the absorbing Markov chain can be defined. Let $\mathbf{N}^t$

be the fundamental matrix for the packet, which is generated at time slot t and has the $TTL = k$. $\mathbf{N}^t$ is calculated as:

$$\mathbf{N}^t = \mathbf{I} + \sum_{i=t}^{t+k-1} \prod_{j=t}^{i} \mathbf{Q}_{j-t}^{j} \tag{4.13}$$

where $\mathbf{I}$ is the identity matrix. $\mathbf{N}^t$ is a $n^{TR} \times n^{TR}$ matrix whose element $n_{n,m}^t$ is the expected number of times the network is in state m, starting from state n, before getting absorbed. Therefore, the sum of a row in matrix $\mathbf{N}^t$ is the expected number of steps until absorption, when starting from the respective state at time slot t.

Now, the absorbing probabilities matrix can be obtained. $\mathbf{B}^t$ is defined as the absorbing probabilities matrix for packets, which are generated at time slot t. $\mathbf{B}^t$ is calculated as:

$$\mathbf{B}^t = \frac{1}{k} \sum_{i=t}^{t+k-1} (\mathbf{N}^t \times \mathbf{R}_{i-t}^{i}) \tag{4.14}$$

where each element $b_{n,m}^t$ is the probability of being absorbed in an absorbing state m during k time slots, given that we start at a transient state n.

We assume that the initial network state is one of the state in $\mathbb{S}^{TR}$. When source node u generates packet p at time slot t, the network state is $X = (0, 0, ..., x_u = 1, ..., 0, 0)$. Let $p_t^I(Z)$ be the probability that the initial network state is state Z ($Z \in \mathbb{S}^{TR}$). In our model, $p_t^I(Z)$ is set to $p(X, Z)_t$, with $t_p = k$.

Let $p_d(X^*)$ denote the probability that the final network state is absorbing state X^*. From the probability that the initial network state is state $X \in \mathbb{S}^{TR}$ and the probability of being absorbed in state X^*, given that the initial state is state X, $p_d(X^*)$ is obtained as:

$$p_d(X^*) = \frac{1}{36} \sum_{t=1}^{36} \sum_{X \in \mathbb{S}^{TR}} (p_t^I(X) \times b_{X,X^*}^t) \tag{4.15}$$

where $p_d(X^*)$ is the average value of 36 time slots in a day.

Now, PDR of packets from source node u to the destination v is denoted by p_d. $p_d(X^*)$ is calculated for all $X^* \in \mathbb{S}^{AB}$. Then, p_d is the sum of those values.

$$p_d = \sum_{X^* \in \mathbb{S}^{AB}} p_d(X^*) \tag{4.16}$$

In order to obtain the delivery latency, first, assume that the network ends up absorbing

state X^*. Now, there is only one absorbing state in the set of absorbing states (i.e., state X^*). The set of transient states is also updated. Specifically, states that are impossible to switch to X^* are removed. Let $\mathbb{S}^{AB}_{X^*}$ and $\mathbb{S}^{TR}_{X^*}$ denote the set of absorbing states and the set of transient states for this case, respectively. All conditional transition probabilities, given that the process ends up in state X^* are computed to update $p^I_t(X)$. $\mathbb{Q}^t$ and $\mathbb{R}^t$ are also updated based on those probabilities. A new fundamental matrix $\mathbf{N}^{t*}$ is obtained for new transition matrices. Let the vector $N^{t*}_i = (n^{t*}_{i,1}, n^{t*}_{i,2}, ..., n^{t*}_{i,n^{TR}})$ denote the row i^{th} in matrix $\mathbf{N}^{t*}$. The expected number of steps until absorbing state X^*, when starting at state i is defined as δ^t_{i,X^*}, whose value is the sum of all elements in N^{t*}_i. The values of δ^t_{i,X^*} are obtained for all absorbing state $X^* \in \mathbb{S}^{AB}$.

Let τ be the duration of a time slot. Note that each step corresponds to a time slot. ED is defined as the delivery delay of packets from source node u to destination v. Then, ED is computed as:

$$ED = \tau \times \frac{1}{36} \sum_{t=1}^{36} \sum_{X^* \in \mathbb{S}^{AB}} \left(\frac{p_d(X^*)}{p_d} \sum_{X \in \mathbb{S}^{TR}_{X^*}} (p^I_t(X) \times \delta^t_{i,X^*}) \right) \tag{4.17}$$

where using the initial probabilities, $p^I_t(X)$, and the law of total expectation, ED is obtained and it is also the average value for 36 time slots in a day.

4.3.4 Comparing with the Simulation

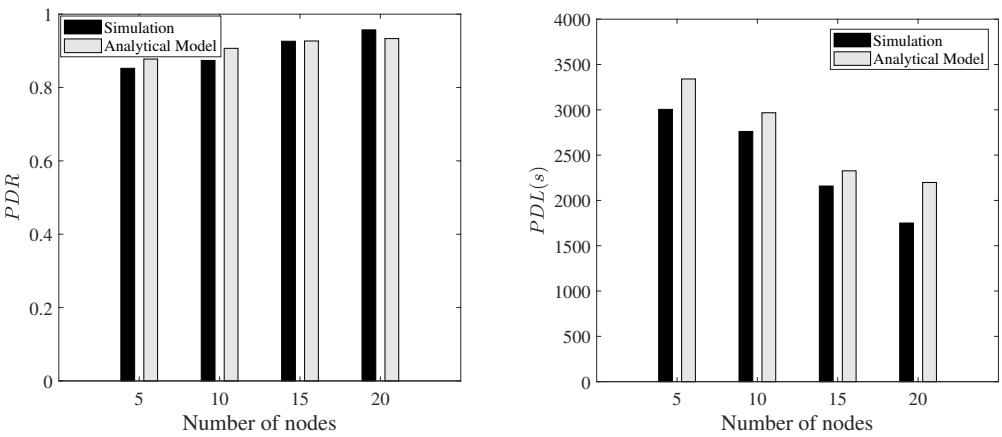

(a) PDR. (b) PDL.

Figure 4-3: The results from the analytical model and the simulation with the various number of nodes in the network

In this subsection, the analytical model is compared with the simulation. First, a part of Helsinki map [78], with a size of $2,000$ meter $\times$ $2,000$ meter was used for the simulation. We generate the movements of 20 nodes for 100 days by using the social relationship-aware human mobility model (SRMM) [79], which reflects the characteristics of human movement (i.e., flight lengths, inter-contact times, the radius of gyrations, and pause times) and the social context. In SRMM, people are partitioned into social groups based on information from a social graph. People in the same group have several common places where they frequently visit. Then, the movements of the people are determined by considering the distances from people to places, and social relationships between people. For instance, people prefer visiting nearby places, as well as places where many of their friends are. In SRMM, people are assumed to move 12 hours per day. The movements from day 1 to day 98 were used to obtain the meeting probability between nodes in the network. The simulations of routing protocols were performed on days 99 and 100 with 24 hours simulation time and an opportunistic networking environment (ONE) simulation tool [78] was used.

The TTL is set to 3 hours ($k = 9$ time slots). The initial value of forwarding token C is 4. κ and χ are set to 0.6 and 0.5, respectively. The packet generation interval is randomly set at between 25 and 30 seconds.

One source and destination pair is randomly chosen for simulation. The result is the average over five-times simulations with five different pairs of source and destination. The analytical model also obtains the results for five pairs of source and destination, respectively.

Figure 4-3 shows the network performance obtained from the analytical model and the simulation with the various number of nodes in the network. The results of PDR are presented in Figure 4-3(a). For a larger number of nodes in the network, packets have more chances to forward to a better relay, which leads to a higher PDR. That is reflected in both the analytical model and the simulation. Specifically, Figure 4-3(a) indicates that PDR increases as the number of nodes increases. Overall, the obtained results show that PDR from the analytical model coincides well with the simulation.

Figure 4-3(b) shows the results of PDL. The trends between the analytical model and the simulation match. Specifically, PDL was reduced when the number of nodes increased since, with a larger number of nodes, the possibility of meeting and forwarding packets to nodes that have higher meeting probabilities with the destination is increased. Figure 4-3(b) also indicates that PDL, which is obtained by the analytical model, is slightly longer than the simulation results. It is partially because, in the analytical model, each step for state

transition is processed at the end of a time slot. However, in the simulation, packets could be forwarded in the middle of a time slot.

4.4 Performance Study

In this section, the performance of the proposed routing protocol is evaluated in terms of PDR, PDL, and DC. First, TSIRP was validated with three PFMs. Then, TSIRP was compared with epidemic routing [16], the spray-and-wait routing protocol [18], PRoPHET [20], and CORP [21].

4.4.1 Simulation Setup

A map of Helsinki [78], with a size of $8,300$ m $\times$ $7,310$ m was used as the simulation area. Let T denote the simulation time. In this paper, the movements of 150 nodes for 81 days were generated by SRMM. The movements from day 1 to day 80 were used to obtain PFMs in TSIRP and the delivery predictability in PRoPHET and CORP. The simulations of routing protocols were performed on day 81 with simulation time $T = 12$ hours. It is assumed that people move between places by car in the city. Based on car speeds from [80], the speed of node movement was set to follow a normalized distribution: $N(39, 5^2)$ km/h.

We used the media access control (MAC) layer of Bluetooth 5.0 with a node transmission range of 100 m, and a transmission rate of 2 Mbps. Packets were generated with a size of 500 bytes, and the generation interval was randomly set at between 25 and 30 seconds. The TTL for packets was set to three hours. Each node has a buffer that can store 100 packets. The initial value of forwarding tokens C and χ were set to 32 and 0.5, respectively. In our simulation, a message can contain different information (e.g., an emergency alert, a traffic jam notification, or weather information). Depending on the information a message carries, the message should have a different value for d_t, which determines whether the message is experiencing a long delay or not. Therefore, the values of time threshold d_t were assumed to be $N(80, 10^2)$ minutes.

In addition, we also compared the proposed protocol with other routing protocols. Common parameters, such as the network area, the number of nodes, the mobility model, and the MAC layer were the same in all routing protocols. Under PRoPHET, the initialization constant of delivery predictability, P_{init}, the aging constant, γ, and the scaling constant, β, were set to 0.75, 0.98, and 0.25, respectively. For CORP, the maximum probability threshold P_{max} and minimum probability threshold P_{min} were set to 0.88 and 0.45, respectively.

Under the spray-and-wait, the forwarding token was set to the same value as our routing protocol. A summary of simulation parameters is in Table 4.3.

Table 4.3: Simulation parameters

Parameter	**Value**
Size of network area	8,300 m×7,310 m
Number of nodes (N)	150
Simulation time (T)	12 h
Mobility model	SRMM
The speed of node movement	$N(39, 5^2)$ km/h
MAC layer	Bluetooth 5.0
Transmission rate	2 Mbps
Transmission range	100 m
Packet TTL	3 h
Packet size	500 bytes
Packet generation interval	25-30s
Buffer size	100 packets
Initial value of forwarding token (C)	32
Time threshold for considering the mean value of degree centrality (d_t)	$N(80, 10^2)$ min

4.4.2 Effects of the Spreading Rate Control Threshold (κ) and the Initial Value of the Forwarding Token (C) on the Performance for Three PFMs

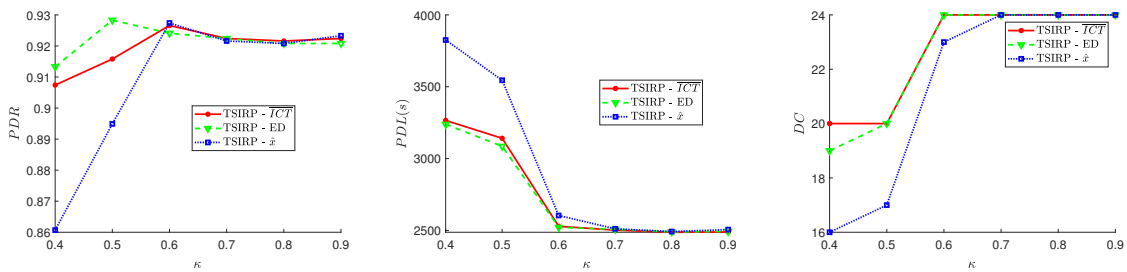

(a) PDR. (b) PDL. (c) DC.

Figure 4-4: The network performance for three PFMs with various κ values (the spreading rate control threshold).

In this subsection, the effects of three potential forwarding metrics ($\overline{ICT}$: the mean value of inter-contact time, ED: the expected delivery delay, $\hat{x}$: the number of time slots to satisfy the meeting probability condition) are analyzed. ED between nodes was computed with $k = 100$ time slots. The required meeting probability, ϑ, was set to 0.2 when we calculated $\hat{x}$. For the three PFMs, network performance based on various values for κ and C was collected.

Figure 4-4 shows the network performance for the three PFMs with various κ values. In Fig. 4-4(a), PDR increased significantly when κ increased from 0.4 to 0.6, and then slightly decreased if κ kept increasing. For a low value of κ, the message spreading rate is quickly reduced and packets are not spread widely enough. In contrast, if κ is large, the relay selection will be performed too late. Those reasons led to a low PDR. As shown in Fig. 4-4(a), the best packet delivery ratio was achieved when $\kappa = 0.6$. For the three PFMs, when $\kappa = 0.4$ and $\kappa = 0.5$, higher packet delivery ratios were obtained by using ED. Then, when κ was between 0.6 and 0.9, different PFMs obtained similar values for PDR.

Figure 4-4(b) illustrates PDL for the three PFMs. Overall, the results indicate that all three PFMs have a lower PDL from a larger value for κ. ED achieved a lower PDL than $\overline{ICT}$ and $\hat{x}$ because, based on temporal social interactions, nodes that have lower values for ED were determined and selected as relay nodes.

The results for DC are displayed in Fig. 4-4(c). It is clear that DC increased to a certain point when κ varied between 0.4 and 0.6, and did not change after that. With a large value for κ (between 0.7 and 0.9), most of the message copies were forwarded to neighbor nodes without considering PFM, so DC was high, and different PFMs obtained similar results.

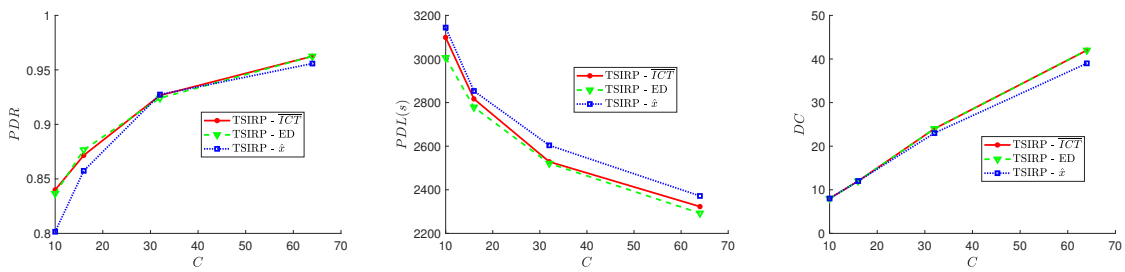

(a) PDR. (b) PDL. (c) DC.

Figure 4-5: The network performance for three PFMs with various C values (the initial value of the forwarding token).

The network performance for the three PFMs with various C values is shown in Fig.

4-5. PDR is presented in Fig. 4-5(a). We see that a larger C value achieves a better packet delivery ratio because, with a large C value, the number of copies of messages in the network was also large, and the messages had a high possibility of being delivered to the destinations. The obtained results with $\overline{ICT}$ and ED are similar and higher than the results with $\hat{x}$. Figure 4-5(b) presents PDL for various C values. Overall, latency decreased when there was an increase in C values; by selecting relay nodes with lower values for ED, PDL based on ED was lower than with the other PFMs.

The results of DC for various C values are displayed in Fig. 4-5(c). As shown in the figures, DC increased as C increased, since a large C value means a large number of message replications. The results obtained for the different PFMs are similar in terms of DC.

Based on the results of network performance in Fig. 4-4 and Fig. 4-5, the value of κ was set to 0.6, and the expected delivery delay (ED) was used as the PFM to compare with other routing protocols.

4.4.3 Effects of the Packet Generation Interval on the Performance of Routing Protocols

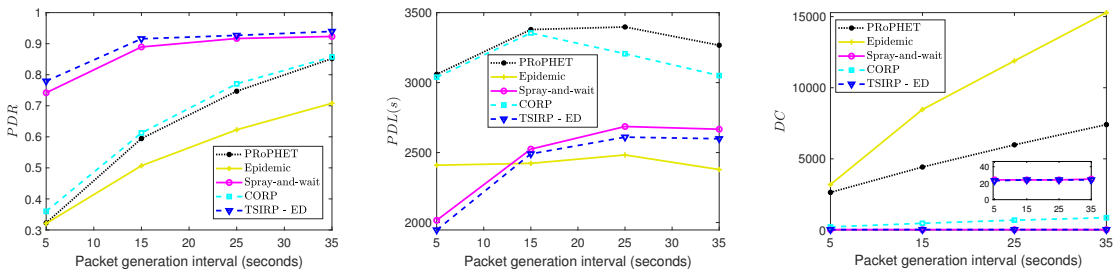

(a) PDR. (b) PDL. (c) DC.

Figure 4-6: The network performance for various values of the packet generation interval.

The network performance for various values of the packet generation interval is presented in Fig. 4-6. PDR is shown in Fig. 4-6(a). We see that all five protocols achieved higher packet delivery ratios as the packet generation interval increased since the network traffic is lower with a longer packet generation interval. By controlling the message spreading rate and selecting relay nodes with lower values for ED, PDR under TSIRP is higher than the others. In PRoPHET and epidemic routing, the message spreading rate was not considered, and the number of replications was not limited. Thus, the buffer filled, and a lot of packets were dropped, which led to a low value for PDR. By using the network

community information, PDR in CORP is higher than those in PRoPHET and epidemic routing. In the spray-and-wait routing protocol, by limiting the number of replications, the buffer overflow was reduced and PDR was greater than that in CORP.

Latency from various values for the packet generation interval is illustrated in Fig. 4-6(b). Based on the flooding strategy, epidemic routing provided a shorter delay than other routing protocols with less network traffic (i.e., a longer packet generation interval). Under TSIRP and the spray-and-wait routing protocol, PDL increased when we increased the packet generation interval because, with a short packet generation interval, the network traffic is heavy and the buffer overflows. Therefore, when new packets are generated and received, packets with long delays are removed from the buffer to store the new packets. As a result, there are only packets with short delays in the buffer. That creates low values for PDL. When the packet generation interval is longer, buffer overflow is reduced, and more packets with longer delays are in the buffer, which increases latency. Under PRoPHET and CORP, when a message has just been generated, the message is slowly spread due to nodes performing relay selection. Therefore, PDL under PRoPHET and CORP is long. By controlling the message spreading rate, TSIRP resolves this problem, and nodes with lower values for ED are preferred as relay nodes. That reduces the latency. As shown in Fig. 4-6(b), TSIRP achieved a lower latency than PRoPHET and the spray-and-wait routing protocol.

Figure 4-6(c) displays the results for DC. Under TSIRP and the spray-and-wait routing protocol, low values for DC were obtained by limiting the number of replications, whereas epidemic routing and PRoPHET had very high values for DC. In the CORP, by finding the node in the destination's community before finding the destination, DC is also reduced. For example, when the packet generation interval is five seconds, DCs from TSIRP, the spray-and-wait routing protocol, and CORP were 23, 24, and 212, respectively, whereas epidemic routing and PRoPHET obtained 3194 and 2643, respectively.

4.4.4 Effects of Packet TTL on the Performance of Routing Protocols

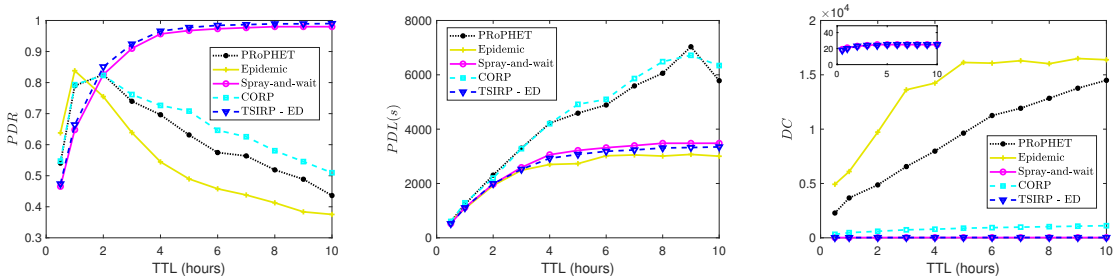

(a) PDR. (b) PDL. (c) DC.

Figure 4-7: The network performance for various values of packet time to live.

In this subsection, we also collect and present the result of epidemic routing in the case of unlimited buffer size for various TTL values to show the theoretical maximal performance and compare it with our routing protocol.

In Fig. 4-7, the network performance for various values of TTL is illustrated. PDR is shown in Fig. 4-7(a). The results indicate that giving a longer lifetime to packets increases PDR up to a certain point, and then, PDR settles under TSIRP and the spray-and-wait routing protocol but decreases in epidemic routing, and PRoPHET due to buffer overflow. In CORP, by trying to forward the packet to the destination's community, the buffer overflow is reduced and PDR is slightly higher than PRoPHET. By considering packet spreading rate and relay selection, PDR from TSIRP is higher than from other routing protocols when TTL varies between 2 hours and 10 hours, and it close to the theoretical maximal value with a large value for TTL (e.g., TTL between 6 hours and 10 hours)

PDL results are in Fig. 4-7(b). A large value for TTL means packets can be stored for a long time in the buffer, which leads to increased latency, as shown in the figure. Epidemic with unlimited buffer size obtained the lowest value. The results also indicate that PDL under TSIRP is lower than under PRoPHET and the spray-and-wait routing protocol, and is slightly longer than epidemic routing.

DC with various values of TTL is presented in Fig. 4-7(c). The obtained results from TSIRP are better than from other routing protocols due to the small number of replications and from executing relay selection. Under PRoPHET and epidemic routing, when TTL increases, a lot of packets are dropped and re-transmitted due to the buffer overflow. In the case of epidemic routing with the unlimited buffer size, the buffer overflow does not happen

and packets are not dropped. That is the reason why DC from PRoPHET and epidemic routing higher than epidemic routing with unlimited buffer.

4.4.5 Effects of Buffer Size on the Performance of Routing Protocols

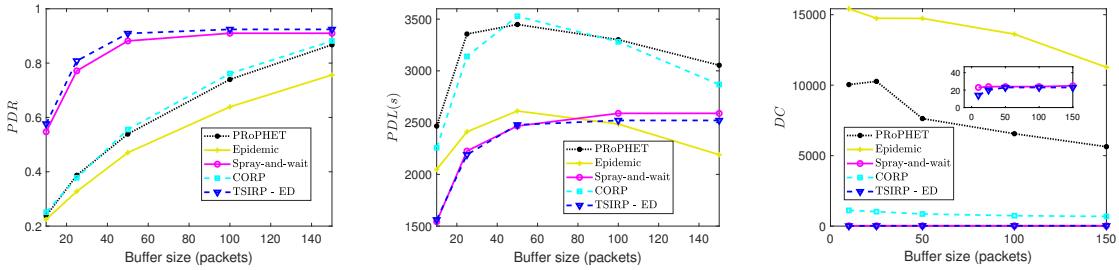

(a) PDR. (b) PDL. (c) DC.

Figure 4-8: The network performance for various buffer sizes.

Figure 4-8 displays the network performance for various buffer sizes. First, PDR is shown in Fig.4-8(a). We can see that PDR increased as the buffer size increased since a large buffer means more packets can be forwarded and stored in it. PDR in CORP is higher than PRoPHET and lower than the spray-and-wait routing. TSIRP always achieves the best packet delivery ratio with the various buffer sizes.

PDL is in Fig. 4-8(b). When the buffer size is smaller than 100 packets, the proposed routing protocol delivered lower latency than the others. Note that a shorter latency was achieved under epidemic routing when the buffer size increased to 150 packets since a large buffer will reduce the packet loss rate in epidemic routing. However, with epidemic routing, DC is huge, as shown in Fig.4-8(c), because of flooding.

4.5 Chapter Summary

In this Chapter, we proposed an efficient routing protocol for opportunistic mobile networks. Based on temporal social interactions and the history of social interactions between nodes, three PFMs were proposed for relay selection (i.e., the mean value of inter-contact time between nodes, the expected delivery delay, and the number of time slots to satisfy the meeting probability condition). In addition, a scheme to control the message spreading rate was proposed based on the state of the message in order to achieve a balance between PDL and DC. Specifically, based on the residual lifetime and the forwarding token, a spreading rate control value was proposed to control the message spreading rate. This scheme allows

reducing both latency and DC. Furthermore, in our forwarding scheme, if a packet is experiencing a long delay, degree centrality is also used to create more chances to deliver the packet to the destination. In addition, we design an analytical model to study the proposed routing algorithm and the proposed model can accurately estimate the network performance in terms of PDR and the delivery delay.

The human movements generated from SRMM is used for validating TSIRP. The network performance under TSIRP was evaluated by comparing it with other routing protocols (epidemic routing, spray-and-wait, PRoPHET, and CORP) in terms of PDL, PDR, and DC. The simulation results indicate that TSIRP can outperform existing routing protocols.

Chapter 5

Human Location Prediction-Based Routing Protocol

5.1 The Network Model and Problem Definition

In this work, we extend the thesis by studying scenarios for urban sensor networks. Then, a human location prediction model is designed and a human location prediction-based routing protocol is proposed. This section first describes the network model is described. Then, the problem definition is presented.

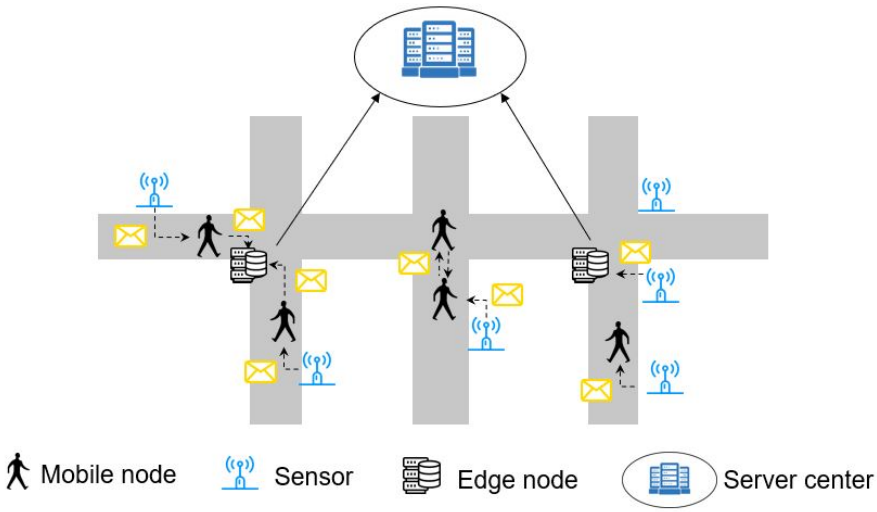

Figure 5-1: The network model.

Figure 5-1 shows the network model that consists of four entities as follows:

- Mobile nodes (mobile users): Mobile nodes collect data, such as temperature, images

of traffic conditions, and videos of accidents, using the sensors embedded in their smart devices (e.g., camera, microphone, positioning sensor, temperature sensor), and send to edge nodes. They can walk or be in a vehicle to move around the area. When mobile users are in contact with other people or sensors, they can exchange data between them and transmit data to the destination.

- Sensors: Sensors are deployed in specific locations to collect data, such as air quality, radioactivity, noise levels, and humidity levels. When sensors and destinations (edge nodes) are not directly connected, the sensors must relay packets to mobile users to transfer them to the destinations.

- Edge nodes: Edge nodes are located in particular locations to gather and preprocess collected data from sensors and mobile users. Then, edge nodes send processed data to the server center.

- The server center: The server center receives data from edge nodes and uses the received data for urban-sensing applications.

Messages in this network can be of different data types, such as text, images, and video. This model could be used in various applications, such as environmental monitoring [23,24], smart traffic light systems [25], and waste management [81]. For example, in monitoring environmental conditions [23,24], the data from sensors, such as air quality, noise, and radiation sensors, and the data from sensors embedded in smart devices for temperature measurement, are collected and sent to edge nodes. Then, edge nodes preprocess the collected data and send it to the server center.

In this system, edge nodes connect with the server center via an infrastructure network, whereas edge nodes, sensors, and mobile nodes exchange messages with each other using wireless communications such as Bluetooth 5.0. Therefore, this work addresses the problem of how to effectively route data from sensors and mobile nodes to edge nodes. Data collection at edge nodes in this system relies on mobile nodes that move around the city. The selection of nodes for forwarding messages is an important issue. Our work considers network performance in terms of DC, PDL, and PDR.

We assume that the movement histories of a number of mobile nodes are observed, and each node knows its encounter history with other nodes. The information from observed movement history is denoted as M. Let $\mathbb{S}_u^{NB}$ denote the set of neighboring nodes of node u. The information on the encounter history of nodes in $\mathbb{S}_u^{NB}$ is denoted E. Node u wants to

send a message to edge node v. The objective is to choose relay nodes in $\mathbb{S}_u^{NB}$ to maximize PDR and minimize PDL and DC, given the information on movement history M and information on encounter history E.

5.2 HLPRP routing protocol

In this section, the proposed human location prediction model is described in detail. Then, we discuss how to determine packet delivery predictability using the estimated information from the human location prediction model. The of nodes is also calculated using their encounter histories. Finally, a forwarding algorithm is proposed based on those metrics. The routing process of HLPRP is shown in Figure 5-2.

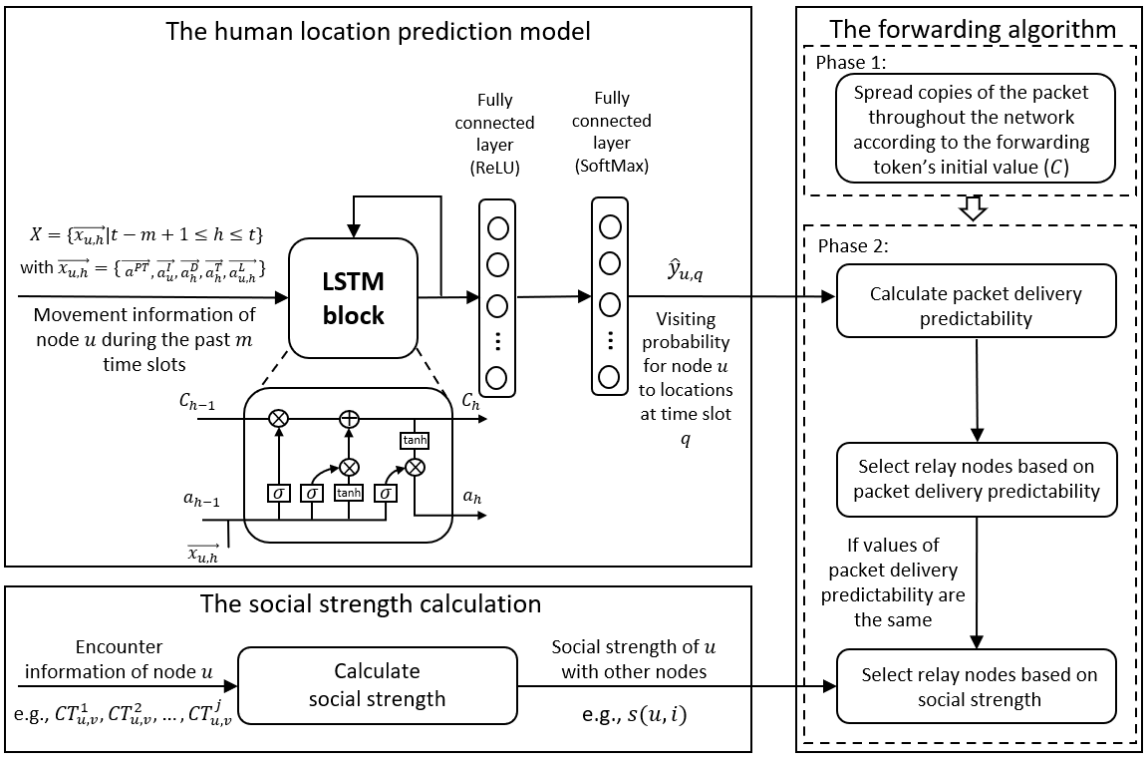

Figure 5-2: The HLPRP routing process.

5.2.1 Human Location Prediction (HLP) Model

We propose a human location prediction model based on a RNN and LSTM cells [28] for estimating mobile users' next positions, using information from their previous movements. In particular, the proposed model takes movement information of mobile users in current and previous time slots as input and outputs estimated locations for the next k time slots.

The information that will be used as input for the prediction model is discussed next. First, to distinguish mobile users, each one is assigned a unique ID. Then, a one-hot vector is used to represent the user ID. Let $\overrightarrow{a_u^I}$ denote the one-hot vector that indicates the ID of user u. Second, a time slot index is also used as an input feature. The one-hot vector that represents time slot h is denoted $\overrightarrow{a_h^T}$. Third, the day of the week is considered. Let $\overrightarrow{a_h^D}$ be the one-hot vector that indicates the day of the week of time slot h. Fourth, the locations of mobile users are taken into account. The one-hot vector that indicates the location of user u in time slot h is $\overrightarrow{a_{u,h}^L}$. Finally, let t denote the current time slot. From time slot t, the human location prediction model will predict the location of mobile user u in the next time slot, q (e.g., with $k = 4$, q could be time slot $t+1$, time slot $t+2$, time slot $t+3$, or time slot $t+4$). To determine time slot q, a one-hot vector is used. Let $\overrightarrow{a^{PT}}$ denote the time slot in which we want to predict the location of user u. $\overrightarrow{a^{PT}}$ is considered an input feature as well. One-hot encoding is used for all input features because those features are nominal and not ordinal. The input will be information from time slot $(t-m+1)$ to current time slot t. Let us define $\overrightarrow{x_{u,h}}$ as the input vector of user u in time slot h, specifically, $\overrightarrow{x_{u,h}} = \{\overrightarrow{a^{PT}}, \overrightarrow{a_u^I}, \overrightarrow{a_h^D}, \overrightarrow{a_h^T}, \overrightarrow{a_{u,h}^L}\}$.

This model is based on a RNN with LSTM cells. After the last hidden state of the LSTM cell, a fully connected layer with ReLU activation and a fully connected layer with a softmax activation function is used for the output layer. Let $\widehat{y}_{u,q}$ denote the output vector that shows the probability that mobile user u will visit locations in time slot q (e.g., $q = t + 1$). For example, $\widehat{y}_{u,q} = [0.1, 0.05, 0.01, \ldots, 0.3]$ means that in time slot q, the probability of visiting the first location is 0.1; the probability of visiting the second location is 0.05, and so on. The notations used in the human location prediction model are shown in Table 5.1.

Table 5.1: Notations used in the human location prediction model.

Notation	Meaning
$\overrightarrow{x_{u,h}}$	Input vector of user u in time slot h
$\overrightarrow{a^{PT}}$	One-hot vector: the next time slot for prediction of the user's location
$\overrightarrow{a_u^I}$	One-hot vector: the ID of mobile user u
$\overrightarrow{a_h^D}$	One-hot vector: the day of the week of time slot h
$\overrightarrow{a_h^T}$	One-hot vector: presents time slot h
$\overrightarrow{a_{u,h}^L}$	One-hot vector: the location of user u in time slot h
$\widehat{y}_{u,q}$	Output vector

5.2.2 Packet Delivery Predictability

In the network model, edge nodes are deployed at certain locations. Suppose that edge node v is located at a certain location in the area. The probability that a mobile user visits edge node v from time slot $t+1$ to time slot $t+k$ is obtained by using the human location prediction model. Let $p(u,v)_{t+j}$ denote the probability that mobile user u visits edge node v at time slot $t+j$. Based on the visit probability, packet delivery predictability (the possibility that a node will deliver a packet to its destination) can be calculated. Let $DP(u,v)_t$ denote the packet delivery predictability of mobile user u to edge node v in time slot t. $DP(u,v)_t$ is calculated as follows:

$$DP(u,v)_t = \sum_{j=1}^{k} (p(u,v)_{t+j})^{\zeta \times j} \tag{5.1}$$

where a tunable parameter, $\zeta \in (0,1)$, is used to adjust the effect of probabilities based on time. Specifically, with $(\zeta \times j)$, the probability for a time slot in the distant future has less effect on the value of $DP(u,v)_t$ than the probability for a time slot in the near future (e.g., $p(u,v)_{t+2}$ affects $DP(u,v)_t$ less than $p(u,v)_{t+1}$). In other words, a node with a high visit probability in the near future has higher packet delivery predictability than a node with a high visit probability in the distant future. A high $DP(u,v)_t$ value indicates that a message can be delivered from mobile user u to edge node v with high probability and low latency. Therefore, a relay node with high packet delivery predictability is preferable.

5.2.3 Social Strength

Social strength is used to represent the social relationships between nodes in the network. To measure the social strength between nodes, connection characteristics such as encounter frequency [82] and contact duration [83, 84] can be used. In this work, social strength is determined based on contact duration between nodes. During the observation time, nodes that have been in touch for a longer period have a higher social strength. Contacts between nodes are assumed to be collected over a time period, T_C. Let η represent the number of contacts between node u and node v. The duration of the ith contact between node u and node v is defined as $CT^i_{u,v}$. Let $s(u,v)$ denote the social strength between node u and node v. Then, $s(u,v)$ is calculated as:

$$s(u,v) = \frac{\sum_{i=1}^{\eta} CT^i_{u,v}}{T_C} \tag{5.2}$$

From Equation (5.2), we see that the social strength of two nodes is the total contact duration between them over the time period of collecting contacts between nodes. A high value for $s(u,v)$ implies that they have a close relationship and usually encounter each other.

5.2.4 Forwarding Algorithm

The proposed forwarding algorithm, based on packet delivery predictability and social strength, is presented in Algorithm 2. The notations used in the algorithm are defined in Table 5.2.

Table 5.2: Notations used in the proposed forwarding algorithm.

Notation	Meaning
$DP(u,v)_t$	The packet delivery predictability between node u and node v in time slot t
$s(u,v)$	The social strength between node u and node v
D_u	The degree centrality of node u
c^p_u	The forwarding token of node u for packet p
$\mathbb{S}^{NB}_u$	The set of neighboring nodes of node u

Assume that node u wants to send packet p to edge node v. First, the neighboring nodes of node u are checked. If the destination is listed in the neighboring nodes, the packet

Algorithm 2 The forwarding algorithm.

1: Node u has packet p to send to edge node v
Input: $\mathbb{S}_u^{NB}, DP(u,v)_t, s(u,v), \zeta, D_u, c_u^p$
2: **for each** $i \in \mathbb{S}_u^{NB}$ **do**
3: **if** $c_u^p > 1$ **then**
4: Node u selects node i as a relay node and forwards a copy of packet p to i
5: $c_i^p = \min(\max(c_u^p \times \frac{D_i}{D_i+D_u+\epsilon}, 1), c_u^p - 1)$
6: $c_u^p = c_u^p - c_i^p$
7: **else if** $c_u^p = 1$ **then**
8: **if** $DP(i,v)_t > DP(u,v)_t$ **then**
9: Node i is chosen as a relay node for packet p
10: **else if** $DP(i,v)_t = DP(u,v)_t$ and $s(i,v) > s(u,v)$ **then**
11: Node i is chosen as a relay node for packet p
12: **end if**
13: **if** Node i is chosen as a relay node for packet p **then**
14: Node u forwards packet p to node i and deletes packet p from buffer
15: $c_i^p = 1$
16: **end if**
17: **end if**
18: **end for**

is delivered to the destination. Otherwise, the forwarding process is executed following Algorithm 2.

In the forwarding algorithm, a forwarding token for packets is used to limit the number of copies of packets in the network similarly in [18,22]. Specifically, when a node generates a packet, it also assigns a forwarding token to the packet. The forwarding token's initial value is C. Let c_u^p represent the forwarding token for packet p of node u. The forwarding algorithm is processed in two phases based on the value of c_u^p. In phase 1, i.e., when $c_u^p > 1$, packets are quickly spread in the network, and degree centrality is used to update the forwarding token's value. In phase 2, when $c_u^p = 1$, relay nodes are selected based on packet delivery predictability and social strength.

Specifically, in phase 1 when $c_u^p > 1$, node u selects node i in $\mathbb{S}_u^{NB}$ as a relay node and forwards a copy of packet p to node i without consideration of any other condition in line 4. Based on the social strength between nodes, a social graph is constructed. In the social graph, vertices are nodes, and there is a link between two nodes if their social strength is greater than zero. The degree centrality of a node is defined as the number of links between itself and other nodes in the social graph. To update the forwarding token's value, degree centrality is used. Let D_u and D_i represent the degree centrality of node u and the degree centrality of node i, respectively. The forwarding token's value assigned to the copy of packet

p at node i is denoted as c_i^p, which is calculated as follows:

$$c_i^p = \min(\max(c_u^p \times \frac{D_i}{D_i + D_u + \epsilon}, 1), c_u^p - 1) \tag{5.3}$$

where a very small value, ϵ, is added to avoid the denominator being zero. According to Equation (5.3), c_i^p is limited to values between $[1, c_u^p - 1]$, and a node with a larger value for the degree centrality will be assigned a greater forwarding token's value. In the real context, a node with a high degree of centrality has a greater likelihood of connecting with other nodes. If it has a large value for the forwarding token, copies of the packet will quickly spread throughout the network. That supports minimizing PDL and enhances the possibility of delivering the packet to its destination. In Algorithm 2, c_i^p is calculated in line 5, and c_u^p is updated in line 6 (i.e., $c_u^p = c_u^p - c_i^p$).

In phase 2, when $c_u^p = 1$, the packet delivery predictabilities are compared in line 8. If node i has a greater packet delivery predictability with edge node v than node u (i.e., $DP(i,v)_t > DP(u,v)_t$), node i is chosen as a relay node for packet p in line 9. Otherwise, if $DP(i,v)_t = DP(u,v)_t$, social strengths are compared in line 10. Specifically, if $DP(i,v)_t = DP(u,v)_t$ and $s(i,v) > s(u,v)$, node i is selected as a relay node for packet p in line 11. Finally, if node i is chosen as the relay node for packet p, node u will forward packet p to node i and delete packet p from its buffer (line 14). The forwarding token's value for packet p at node i, c_i^p, is set to 1 (line 15).

5.3 Performance Evaluation

In this section, first, a Wi-Fi scan dataset is presented. Then, the simulation setup is discussed. The results of the proposed HLP model are presented and compared with the results of the Markov model [85]. The performance of the proposed routing protocol is evaluated in terms of DL, PDL, and DC. The proposed routing is compared with epidemic routing [16], the spray-and-wait routing protocol [18], PRoPHET [20], CORP [21], and TSIRP [22]. The opportunistic networking environment (ONE) simulation tool [78] is used for simulation.

5.3.1 Dataset

The UB/phonelab-wifi logs were gathered over a five-month period from the smartphones of 284 faculty members, staff, and students at the University at Buffalo [86]. We specifically

use the sub-dataset named WifiScanResult, which includes the Wi-Fi scan records of 274 anonymous mobile users and about 1.1 million access point (AP) scans. When a phone scans for and finds a nearby AP, it records information, such as the timestamp, device ID, basic service set identifier (BSSID), and signal strength. Most people carry their phones, and indoor Wi-Fi APs often have short transmission ranges of tens of meters. Thus, the human movement could be represented as a sequence of scanned APs identifiable by their BSSIDs [87]. A smartphone can scan and detect several APs at one time. The scanned AP with the highest signal strength is chosen to reflect mobile users' positions.

We focus on data collected over 90 days from 1 January to 31 March 2015. During this period, the most Wi-Fi activities for all selected mobile users, as well as their interactions, can be observed. Then, the 50 most active users and 1243 of the most visited APs are chosen as input data for building our proposed human location prediction model. An extra dummy AP is added for a time slot in which there are no scanned APs. The proposed model estimates mobile users' locations from 9 a.m. to 6 p.m. (the most active period of the day). Therefore, to train the model, human movement from 8 a.m. to 6 p.m. is extracted. Specifically, the time period from 8 a.m. to 6 p.m. is divided into 41 time slots of 15 minutes (including the last time slot from 6 p.m. to 6:15 p.m.), and then, each data sample's timestamp is mapped to one of the predefined 41 time slots. During a time slot, the latest position of the user is considered the user's position for that whole time slot.

Because the UB dataset is sparse, there are a lot of dummy labels. To prevent the model from predicting the dummy location as the next location, all training and validation samples containing dummy labels are removed. Note that only dummy locations from the label are removed, allowing for the possibility of dummy locations in input samples. Following the data extraction procedures mentioned above, we derive a new dataset from which to build the proposed human location prediction model.

5.3.2 Simulation Setup

The data for 13 February 2015, is used to simulate the proposed routing protocol. The remaing 89 days are used to train and test the human location prediction model. The simulation's duration is set to nine hours (i.e., from 9 a.m. to 6 p.m.). The number of edge nodes and the number of sensors are set to 5 and 50, respectively. These nodes are randomly placed at locations of frequently scanned APs. Specifically, from 20 access points (APs) that have the highest number of scanned times by mobile users, five APs are randomly selected

as locations to deploy five edge nodes. From 150 APs that have the highest number of scanned times by mobile users, 50 APs are randomly selected as locations to deploy sensors. Using this method, the edge nodes and the sensor nodes are deployed to locations that are frequently visited by mobile nodes. In other words, they are deployed at locations with a high density of mobile users. Note that in order to reflect a more realistic scenario in this work, a scenario in which some of the users have predictable mobility and the rest have unpredictable mobility is considered. Therefore, the 50 most active users were selected from the UB dataset and were considered users with predictable mobility. The human location prediction model is trained and tested using the movement history of those people. Thus, their future locations can be predicted using the model. Moreover, we also select 100 additional mobile users from the UB dataset and assume that they have no movement history. The locations of those nodes are unpredictable. Therefore, their packet delivery predictability is set to zero. However, in the network model, it is also supposed that each node knows its encounter history with other nodes. Therefore, the social strength of those 100 mobile users can still be determined. Finally, the total number of mobile nodes is 150 (i.e., 50 mobile users with movement history and 100 mobile users without movement history).

The media access control (MAC) layer of Bluetooth 5.0 with a transmission rate of 2 Mbps is used. Bluetooth 5.0 is designed for very low power operation. That reduces power usage and extends battery life for nodes. The UB dataset provides the Wi-Fi scan records of mobile devices. Indoor Wi-Fi APs often have short transmission ranges of tens of meters. There is no physical location information for APs and mobile users in the UB dataset. The real distance between nodes cannot be obtained. Therefore, we assume that a mobile user communicates with another mobile user if they scan and detect at least one common AP. In addition, a mobile user communicates with a sensor or an edge node if the user scans and detects the AP where the sensor or the edge node is placed. Packets are generated with a size of 500 bytes (e.g., the size of sensing data or a text message), and the generation interval is randomly set at between 25 s and 30 s. We consider the network model that allows messages with a long expiration time. Therefore, the time to live (TTL) for packets was set to four hours. Each node has a buffer that can store 150 packets. The first-in-first-out (FIFO) buffer is used. The initial value of forwarding token C is set to 64. In addition, the proposed protocol is also compared with other routing protocols. Common parameters, such as the number of nodes and the MAC layer are the same in all routing protocols. The forwarding token under spray-and-wait and TSIRP is set at the same value in HLPRP. In TSIRP, the

expected delivery delay (ED) is used as potential forwarding metric. Under PRoPHET, first, the initialization constant of delivery predictability, P_{init}, was set to 0.75. Then, the scaling constant, β, and aging constant, γ, were set to 0.25 and 0.98, respectively. For CORP, the threshold of minimum probability and the threshold of maximum probability are set to 0.45 and 0.88, respectively. Table 5.3 shows the details for the simulation parameters.

Table 5.3: Simulation parameters.

Parameter	**Value**
Simulation duration	9 h
Number of edge nodes	5
Number of sensors	50
Number of mobile users with movement history	50
Number of mobile users without movement history	100
Transmission rate	2 Mbps
Packet generation interval	25–30 s
Buffer size	150 packets
Packet TTL	4 h
Packet size	500 bytes
Initial value of forwarding token (C)	64

5.3.3 The Results of the Proposed Human Location Prediction Model

Table 5.4 presents the top-1 accuracy of the prediction models when predicting users' locations in various future time slots (i.e., $t+1, t+2, t+3, t+4$). In general, our proposed model obtains higher accuracy than the Markov model. Top-1 accuracy achieves the highest value when predicting the users' locations in the next time slot, $t+1$, and then decreases slightly at time slots in the further future. This indicates that the movement history of mobile users has a greater impact on their locations in the near future than on their locations in the further future. The average accuracy from the proposed HLP model is 0.5831. This indicates that the proposed model can work well. Using the predicted information, the values of packet delivery predictability are obtained for the routing algorithm.

Table 5.4: Top-1 accuracy from the prediction models.

Prediction Model	Time Slot $t+1$	Time Slot $t+2$	Time Slot $t+3$	Time Slot $t+4$	Average
The proposed HLP model	0.6102	0.5907	0.5735	0.5555	0.5831
The Markov model	0.6030	0.5636	0.5338	0.5097	0.5535

5.3.4 Effects of ζ on the Performance of the Proposed Routing Protocol

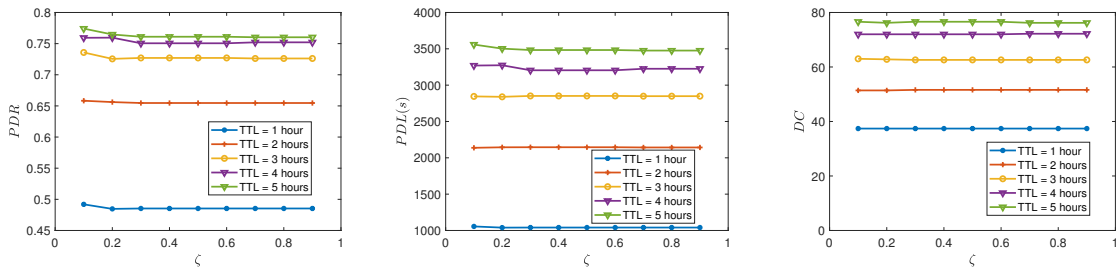

(a) PDR. (b) PDL. (c) DC.

Figure 5-3: The network performance for various values of ζ.

In this subsection, the effects of ζ on the performance of HLPRP are discussed. Recall that when calculating packet delivery predictability, we can adjust the effect on packet delivery predictability of the predicted information for the near future and the distant future by using tunable parameter ζ. Figure 5-3 shows the network performance for various values of ζ and TTL. PDR is shown in Figure 5-3a. In general, PDR is higher with a longer TTL. For the same value of TTL, PDR does not change much. For example, with $TTL = 4$ h, it reduces slightly when ζ increases from 0.1 to 0.3, and then it slightly increases from 0.7506 to 0.7521 when ζ increases from 0.6 to 0.7. Figure 5-3b displays PDL. PDL increases when the TTL increases. For low values of ζ, latency is high. Then, it decreases when ζ increases. For example, with the $TTL = 4$ h, PDL is 3269 s when $\zeta = 0.1$ and 3225 s when $\zeta = 0.7$. DC is presented in Figure 5-3c. DC is larger with a longer TTL. The value of ζ does not affect DC much. It is similar for the various values of ζ. For example, DC is 37.4 when the $TTL = 1$ h for all different values of ζ.

From the obtained results in Figure 5-3, the value of ζ was set to 0.7 in the proposed routing protocol.

5.3.5 Effects of Packet TTL on the Performance of Routing Protocols

Figure 5-4 shows the network performance for various TTL values. First, the results for PDR are presented in Figure 5-4a. Overall, the figure shows that increasing the lifetime of packets increases PDR to a certain point, and then it stabilizes under HLPRP, CORP, TSIRP, and spray-and-wait routing protocols but decreases under epidemic routing and PRoPHET. CORP tries to forward the packet to the community of the destination. In a sparse network, nodes belonging to two distinct communities rarely communicate with one another. Hence, there are very few nodes that can be selected as relay nodes. As a result, CORP obtained the lowest values for the PDR. The number of packet copies was not limited in PRoPHET and epidemic routing. Thus, the buffer quickly filled when the TTL increased, and a large number of packets were dropped, resulting in a low value for PDR. For example, PDR of PRoPHET reduces from 0.6874 to 0.5363 when the TTL increases from 3 h to 6 h. In the spray-and-wait routing protocol, buffer overflow was reduced by the limited number of replications. Therefore, PDR of the spray-and-wait is greater than that of PRoPHET and epidemic routing. By limiting the number of copies of packets, TSIRP and HLPRP can also reduce buffer overflow. TSIRP achieves high values of PDR with using PFM. In HLPRP, relay selection is based on packet delivery predictability and social relationships. Optimal relay nodes can be found, and hence, PDR under HLPRP is improved and is higher than those of the other protocols. For example, when the TTL is 6 h, the PDR of HLPRP, TSIRP, spray-and-wait routing, PRoPHET, CORP, and epidemic routing are 0.7645, 0.7591, 0.7450, 0.5363, 0.4371, and 0.4074, respectively.

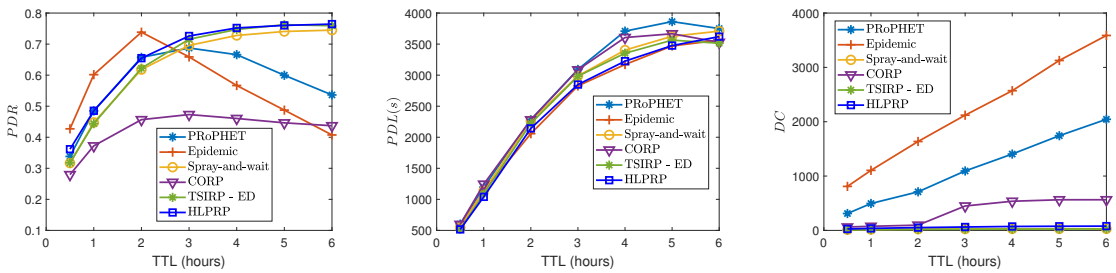

(a) PDR. (b) PDL. (c) DC.

Figure 5-4: The network performance for various values of packet time to live.

Latency from various values for the packet TTL is illustrated in Figure 5-4b. In general, a larger value for TTL means packets can be stored in the buffer for longer, which leads to an increased PDL, as shown in the figure. Under CORP and PRoPHET, a packet is

slowly spread due to the absence of a rapid packet-spreading mechanism. This results in a significant increase in PDL. Based on the flooding strategy, PDL under epidemic routing is low. In TSIRP, a node with a lower value of ED is preferred as relay. Therefore, PDL is reduced. Under HLPRP, packets are quickly spread during phase 1, and nodes with a higher probability of meeting the destination in a short period of time are preferred as relay nodes during phase 2. Therefore, HLPRP also achieves a short delay, comparable to that of epidemic routing, and shorter than the other protocols. For example, when the TTL is 5 h, PDL of HLPRP, TSIRP, and epidemic routing are 3476 seconds, 3563 seconds, and 3470 seconds, whereas spray-and-wait routing, PRoPHET, and CORP are 3626 seconds, 3862 seconds, and 3667 seconds, respectively.

Figure 5-4c shows the results for DC. Under PRoPHET and epidemic routing, the number of packet copies is not limited. As a result, DC is extremely high. When the TTL increases, the buffer overflows, and a large number of packets are dropped. That leads to a quickly increasing DC under those protocols. In CORP, by finding the node in the destination's community before finding the destination, DC is reduced. By limiting the number of replications with the spray-and-wait routing protocol and and TSIRP, low values of DC can be obtained. Under HLPRP, the number of copies of a packet in the network is also limited. DC from HLPRP is also reduced and is lower than that from PRoPHET, CORP, and epidemic routing. For example, when the packet TTL is 2 h, DC from HLPRP, TSIRP, the spray-and-wait routing protocol, and CORP are 51.6, 18.8, 22.4, and 96.6, respectively, whereas PRoPHET and epidemic routing reach 709.6 and 1636.2, respectively. HLPRP's DC is greater than TSIRP's because when the forwarding token value is equal to 1, HLPRP continues to forward the packet if a better relay node is found, whereas TSIRP waits until it reaches the destination.

5.3.6 Effects of Buffer Size on the Performance of Routing Protocols

Figure 5-5 shows the network performance for various buffer sizes. First, PDR is presented in Figure 5-5a. A larger buffer means that it can forward and store more packets. Thus, as shown in Figure 5-5a, PDR increases as the buffer size increases. Our routing protocols (i.e., HLPRP and TSIRP) can achieve a greater PDR than others when the buffer size is between 10 and 250 packets. When the buffer size is very large, buffer overflow is reduced in the flooding strategy. Specifically, epidemic routing obtains high values for PDR when the buffer capacity is larger than 300 packets. However, the flooding strategy also consumes

a significant amount of network resources.

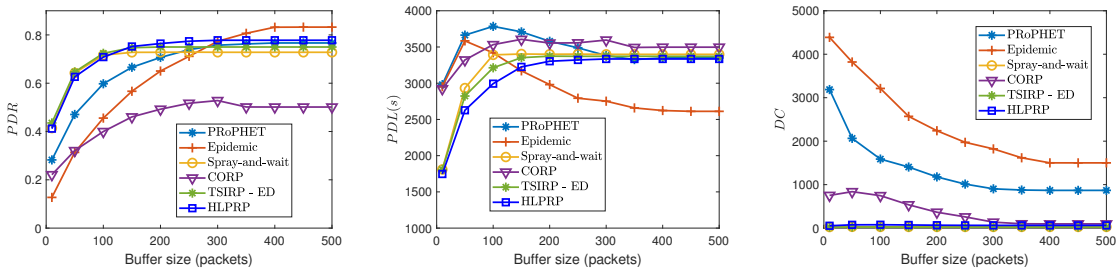

(a) PDR. (b) PDL. (c) DC.

Figure 5-5: The network performance for various buffer sizes.

PDL results are in Figure 5-5b. A small buffer (e.g., 10 packets) will quickly overflow. As a result, it removes packets with long delays to make room for the new ones coming. Therefore, the buffer contains only packets with short delays. This results in low PDL. When the buffer size increases, it can contain more packets with longer delays, which increases latency. By using the predicted information and the social strength between nodes, the shortest latency is obtained by HLPRP when the buffer capacity is between 10 and 100 packets. In epidemic routing, a large buffer can store more packets. Packets are quickly sent to their destinations without being dropped. Hence, epidemic routing with a large buffer (e.g., 300 packets) has a short PDL.

Figure 5-5c shows the results for DC. When the buffer is small, numerous packets are lost and retransmitted due to buffer overflow under epidemic routing and PRoPHET. That creates a huge DC. DC from HLPRP is lower than that from PRoPHET, CORP, and epidemic routing.

5.3.7 Effects of the Packet Generation Interval on the Performance of Routing Protocols

In Figure 5-6, network performance for various packet generation intervals is shown. The results for PDR are illustrated in Figure 5-6a. In general, increasing the packet generation interval will reduce network traffic. Thus, PDR tends to increase as the packet generation interval increases. By rapidly spreading packets and selecting optimal relay nodes based on the predicted information and social relationships, HLPRP achieves a better PDR than the others when the packet generation interval is between 25 s and 45 s.

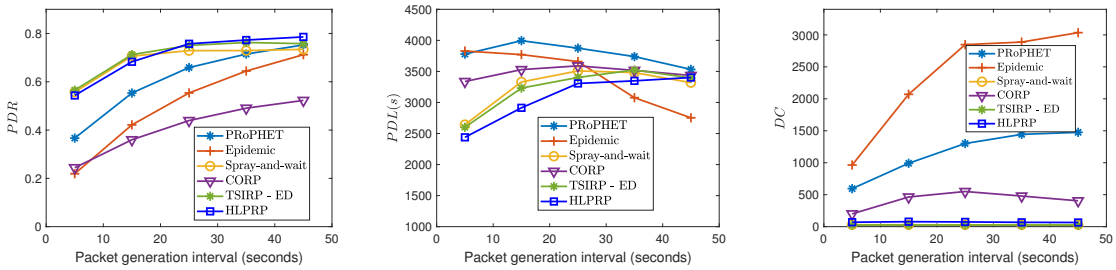

(a) *PDR*. (b) *PDL*. (c) *DC*.

Figure 5-6: The network performance for various values of the packet generation interval.

Figure 5-6b shows the results of *PDL*. The latency from HLPRP is lower than from other routing protocols when the packet generation interval varies between 5 s and 25 s. When network traffic is light (i.e., the packet generation interval is between 35 s and 45 s), using the flooding strategy, epidemic routing obtains the shorter delivery latency. However, *DC* from epidemic routing is huge, as shown in Figure 5-6c. Figure 5-6c also indicates that HLPRP has a lower *DC* than CORP, PRoPHET, BUBBLE Rap, and epidemic routing.

5.4 Chapter Summary

In this Chapter, we proposed a novel routing protocol for mobile crowdsensing-based urban sensor networks based on human location prediction. Specifically, a RNN-based model using LSTM cells was built for estimating the locations of mobile nodes. Useful information, such as nodes' identities, time slots in the day, the day of the week, and node location is extracted from the dataset. That information is used to train and test the prediction model. Packet delivery predictability is proposed by using the probabilities obtained from the prediction model. From the encounter histories of the nodes, social strength between them is also determined and considered in the proposed routing algorithm. Specifically, HLPRP is processed in two phases. In the first phase, the degree centrality is used to determine the forwarding token value of relay nodes. That helps to quickly spread the packets throughout the network. In the second phase, packet delivery predictability and social strength are used to select optimal relay nodes. The network performance under HLPRP was evaluated by comparing it with that of other routing protocols in terms of *PDR*, *PDL*, and *DC*. The obtained results showed that based on the human location prediction, HLPRP is slightly better than TSIRP and outperforms the other routing protocols.

Chapter 6

Concluding Remarks

6.1 Summary of the Contribution

This dissertation investigates problems in opportunistic mobile social networks (OMSNs). We introduced a social relationship−aware human mobility model (SRMM) that can capture both social context and human movement features. The temporal social interaction-based routing protocol (TSIRP) is then built, and SRMM is used to generate people's movements in order to validate the performance of TSIRP. Finally, we expand our work by developing a human location prediction model and proposing a routing protocol based on the human location prediction.

Human movement patterns are important for verifying routing protocol performance. Therefore, we developed the social relationship−aware human mobility model (SRMM), which takes into account both the social relationships and the features of human movements. SRMM uses information from a social graph to divide individuals into social groups. Then, based on the distances and social relationships, people's movements are generated. When compared to other models, the experiment results show that human movements from SRMM more closely match real human movement features and clearly reflect social relationships among individuals.

In the second part of this work, the problem of message exchange in general scenarios of OMSNs is studied and a temporal social interactions-based routing protocol (TSIRP) is proposed. The temporal context of social interactions is first considered. Specifically, during a given time of day, a person frequently connects with certain people. Based on social interactions between nodes, potential forwarding metrics are calculated for each time of the day. This information is used to make forwarding decisions. We also built a novel

strategy for controlling the message spreading rate, allowing us to achieve a balance between packet delivery delay and delivery cost. The network performance of TSIRP was compared to different routing protocols in terms of PDR, PDL, and DC. According to the simulation outcomes, TSIRP outperforms existing routing protocols.

Data transmission challenges in urban sensor networks are also investigated. To solve the challenges, a human location prediction-based routing protocol (HLPRP) has been proposed. In particular, a human location prediction (HLP) model has been developed to estimate the position of mobile nodes. The proposed HLP model is built on a recurrent neural network with long short-term memory cells. Each person's movement history is used in the HLP model to estimate their future locations. Then, using estimated location information from the HLP model, packet delivery predictability is determined and used to select optimal relay nodes. Social strength is also considered for relay selection. HLPRP network performance was evaluated by comparing it to other routing protocols. Based on the results, HLPRP is slightly better than TSIRP and outperforms the other routing protocols.

In summary, the main contributions of this work are as follows:

- We summarized studies related to human mobility models and routing protocols in OMSNs. Then, the limits of existing works are discussed. We formally define three problems: generating realistic human movements, routing protocol in general scenarios of OMSNs, and transmitting data in an urban sensor network.

- For generating realistic human movements, we proposed the social elationship-aware human mobility model, which considers both social relationships and human movement characteristics. SRMM divides people into social groups based on a social graph. Then, people's movements are generated based on distances and social relationships.

- For the second problem, a temporal social interactions-based routing protocol (TSIRP) is proposed. Social interactions are first considered temporally. Potential forwarding metrics are determined based on node-to-node social interactions. This information is used for relay selection. We also developed a novel method for controlling message spreading rate, balancing packet delivery delay and cost. An analytical model with an absorbing Markov chain is also proposed to estimate TSIRP performance.

- For third problem, we proposed a human location prediction-based routing protocol (HLPRP). A human location prediction (HLP) model based on a recurrent neural network with long short-term memory cells is designed to estimate the location of mobile

nodes. Following that, packet delivery predictability is determined using estimated location information from the HLP model and used to select optimal relay nodes. Social strength is also taken into account when relays are chosen.

- Various experiments have been conducted to evaluate the proposed human mobility model and the proposed routing protocols. Specifically, SRMM is evaluated using both the synthetic map and the real road map. The results show that SRMM consistently better reflects human movement and social relationships. TSIRP is then validated using generated human movements from SRMM. HLPRP is evaluated using real traces (e.g., UB datasets). The results show that TSIRP and HLPRP outperform existing routing protocols.

6.2 Future Works

For the human mobility model, SRMM considers social groups in which each person belongs to one social group. However, in the real world, an individual can be a member of multiple social groups, and social relationships are also time-dependent. Thus, to make social contexts more realistic in the mobility model, we plan to use social graphs, in which an individual can belong to multiple social groups, and social relationships will change according to the time of day. Additionally, SRMM does not take into account temporal aspects. For instance, a student has a high probability of visiting classes at the school in the morning. Then, in the afternoon, the student may visit parks or return home. We intend to consider the effects of temporal aspects in our future work.

SRMM focuses on the general movement of people in a city-wide area. However, in each specific scenario, the characteristics of human movement can be different. Therefore, we want to consider the characteristics of human movement and design mobility for people in specific scenarios (e.g., workers in industries, people in parks).

For routing protocols, we want to evaluate the performance of proposed routing protocols in real-world scenarios, such as monitoring environmental conditions (e.g., air quality, noise levels, and humidity levels). Social aspects (e.g., information about nodes with strong social ties) have a high probability of helping in the prediction of human locations in the future. However, it is not taken into account in our current HLP model. We plan to take them into account to develop a highly accurate HLP model. This will support the selection of the optimal relay nodes in the routing protocol. Additionally, we would like

to study a reinforcement learning-based routing protocol in which the agent's action is to select relay nodes based on current state information such as social strength, packet delivery predictability, and spatial information.

Bibliography

[1] E. Hyytia, P. Lassila, and J. Virtamo, "A markovian waypoint mobility model with application to hotspot modeling," in *Communications, 2006. ICC'06. IEEE International Conference on*, vol. 3. IEEE, 2006, pp. 979–986.

[2] E. M. Royer, P. M. Melliar-Smith, and L. E. Moser, "An analysis of the optimum node density for ad hoc mobile networks," in *ICC 2001. IEEE International Conference on Communications. Conference Record (Cat. No.01CH37240)*, vol. 3, 2001, pp. 857–861 vol.3.

[3] M. C. Gonzalez, C. A. Hidalgo, and A.-L. Barabasi, "Understanding individual human mobility patterns," *Nature*, vol. 453, no. 7196, pp. 779–782, June 2008.

[4] I. Rhee, M. Shin, S. Hong, K. Lee, S. J. Kim, and S. Chong, "On the levy-walk nature of human mobility," *IEEE/ACM Transactions on Networking*, vol. 19, no. 3, pp. 630–643, June 2011.

[5] K. Lee, S. Hong, S. J. Kim, I. Rhee, and S. Chong, "SLAW: A new mobility model for human walks," in *IEEE INFOCOM 2009*, April 2009, pp. 855–863.

[6] F. Ekman, A. Keränen, J. Karvo, and J. Ott, "Working day movement model," in *Proceedings of the 1st ACM SIGMOBILE Workshop on Mobility Models*, ser. Mobility-Models '08. New York, NY, USA: ACM, 2008, pp. 33–40.

[7] M. Musolesi and C. Mascolo, "Designing mobility models based on social network theory," *SIGMOBILE Mob. Comput. Commun. Rev.*, vol. 11, no. 3, pp. 59–70, Jul. 2007.

[8] C. Boldrini and A. Passarella, "HCMM: Modelling spatial and temporal properties of human mobility driven by users' social relationships," *Computer Communications*, vol. 33, no. 9, pp. 1056–1074, 2010.

[9] A. Chaintreau, P. Hui, J. Crowcroft, C. Diot, R. Gass, and J. Scott, "Impact of human mobility on opportunistic forwarding algorithms," *IEEE Transactions on Mobile Computing*, vol. 6, no. 6, pp. 606–620, June 2007.

[10] M. Kim, D. Kotz, and S. Kim, "Extracting a mobility model from real user traces," in *Proceedings IEEE INFOCOM 2006. 25TH IEEE International Conference on Computer Communications*, April 2006, pp. 1–13.

[11] H. Zhou, X. Chen, S. He, C. Zhu, and V. C. Leung, "Freshness-aware seed selection for offloading cellular traffic through opportunistic mobile networks," *IEEE Transactions on Wireless Communications*, vol. 19, no. 4, pp. 2658–2669, 2020.

[12] B. Ying, K. Xu, and A. Nayak, "Fair and social-aware message forwarding method in opportunistic social networks," *IEEE Communications Letters*, vol. 23, no. 4, pp. 720–723, 2019.

[13] J. Wu, Z. Chen, and M. Zhao, "Information cache management and data transmission algorithm in opportunistic social networks," *Wireless networks*, vol. 25, no. 6, pp. 2977–2988, 2019.

[14] L. Chancay-Garcıa, J. Sendón-Varela, and P. Manzoni, "Opportunistic networks with messages tracking," *Information Technology and Systems: ICITS 2021*, vol. 1, p. 442, 2021.

[15] X. Fu, H. Yao, O. Postolache, and Y. Yang, "Message forwarding for WSN-Assisted Opportunistic Network in disaster scenarios," *Journal of Network and Computer Applications*, vol. 137, pp. 11–24, 2019.

[16] A. Vahdat and D. Becker, "Epidemic routing for partially-connected ad hoc networks," in *technical report CS-2000-06*, Duke University, 2000.

[17] P. Garg, H. Kumar, R. Johari, P. Gupta, and R. Bhatia, "Enhanced Epidemic Routing Protocol in Delay Tolerant Networks," in *2018 5th International Conference on Signal Processing and Integrated Networks (SPIN)*, 2018, pp. 396–401.

[18] T. Spyropoulos, K. Psounis, and C. S. Raghavendra, "Spray and wait: An efficient routing scheme for intermittently connected mobile networks," in *Proceedings of the 2005 ACM SIGCOMM Workshop on Delay-tolerant Networking*. New York, NY, USA: ACM, 2005, pp. 252–259.

[19] D. V. A. Duong and S. Yoon, "An Efficient Probabilistic Routing Algorithm Based on Limiting The Number of Replications," in *Proceedings of 2019 International Conference on Information and Communication Technology Convergence*, Oct 2019, pp. 562–564.

[20] A. Lindgren, A. Doria, and O. Schelén, "Probabilistic Routing in Intermittently Connected Networks," in *Service Assurance with Partial and Intermittent Resources*. Berlin, Heidelberg: Springer Berlin Heidelberg, 2004, pp. 239–254.

[21] S. Haoran, W. Muqing, and C. Yanan, "A community-based opportunistic routing protocol in delay tolerant networks," in *2018 IEEE 4th International Conference on Computer and Communications (ICCC)*. IEEE, 2018, pp. 296–300.

[22] D. V. A. Duong, D.-Y. Kim, and S. Yoon, "TSIRP: A Temporal Social Interactions-Based Routing Protocol in Opportunistic Mobile Social Networks," *IEEE Access*, vol. 9, pp. 72 712–72 729, 2021.

[23] D. Wu, T. Xiao, X. Liao, J. Luo, C. Wu, S. Zhang, Y. Li, and Y. Guo, "When Sharing Economy Meets IoT: Towards Fine-Grained Urban Air Quality Monitoring through Mobile Crowdsensing on Bike-Share System," *Proc. ACM Interact. Mob. Wearable Ubiquitous Technol.*, vol. 4, no. 2, Jun. 2020.

[24] F. Jiang, Y. Sun, and J. Sha, "Crowd Sensing Urban Healthy Street Monitoring Based on Mobile Positioning System," *Mobile Information Systems*, vol. 2021, 2021.

[25] A. Ali, M. A. Qureshi, M. Shiraz, and A. Shamim, "Mobile crowd sensing based dynamic traffic efficiency framework for urban traffic congestion control," *Sustainable Computing: Informatics and Systems*, vol. 32, p. 100608, 2021.

[26] Z. Jiang, H. Zhu, B. Zhou, C. Lu, M. Sun, X. Ma, X. Fan, C. Wang, and L. Chen, "CrowdPatrol: A Mobile Crowdsensing Framework for Traffic Violation Hotspot Patrolling," *IEEE Transactions on Mobile Computing*, pp. 1–1, 2021.

[27] V. Kutsarova and M. Matskin, "Combining Mobile Crowdsensing and Wearable Devices for Managing Alarming Situations," in *2021 IEEE 45th Annual Computers, Software, and Applications Conference (COMPSAC)*, 2021, pp. 538–543.

[28] A. Sherstinsky, "Fundamentals of Recurrent Neural Network (RNN) and Long Short-Term Memory (LSTM) network," *Physica D: Nonlinear Phenomena*, vol. 404, p. 132306, 2020.

[29] I. Rhee, M. Shin, S. Hong, K. Lee, S. Kim, and S. Chong, "CRAWDAD dataset ncsu/mobilitymodels (v. 2009-07-23)," Downloaded from http://crawdad.org/ncsu/mobilitymodels/20090723, Jul. 2009.

[30] M. McNett and G. M. Voelker, "Access and mobility of wireless PDA users," *SIGMOBILE Mob. Comput. Commun. Rev.*, vol. 9, no. 2, pp. 40–55, Apr. 2005.

[31] J. Scott, R. Gass, J. Crowcroft, P. Hui, C. Diot, and A. Chaintreau, "CRAWDAD dataset cambridge/haggle (v. 2009-05-29)," Downloaded from https://crawdad.org/cambridge/haggle/20090529, May 2009.

[32] A. Stopczynski, V. Sekara, P. Sapiezynski, A. Cuttone, M. M. Madsen, J. E. Larsen, and S. Lehmann, "Measuring large-scale social networks with high resolution," *PloS one*, vol. 9, no. 4, p. e95978, 2014.

[33] D. O. Olguín, B. N. Waber, T. Kim, A. Mohan, K. Ara, and A. Pentland, "Sensible organizations: Technology and methodology for automatically measuring organizational behavior," *IEEE Transactions on Systems, Man, and Cybernetics, Part B (Cybernetics)*, vol. 39, no. 1, pp. 43–55, 2008.

[34] A. Socievole, F. De Rango, and A. Caputo, "Wireless contacts, facebook friendships and interests: analysis of a multi-layer social network in an academic environment," in *2014 IFIP Wireless Days (WD)*. IEEE, 2014, pp. 1–7.

[35] A. Munjal, T. Camp, and W. C. Navidi, "Smooth: A simple way to model human mobility," in *Proceedings of the 14th ACM International Conference on Modeling, Analysis and Simulation of Wireless and Mobile Systems*, ser. MSWiM '11. New York, NY, USA: Association for Computing Machinery, 2011, p. 351–360. [Online]. Available: https://doi.org/10.1145/2068897.2068957

[36] G. Solmaz, M. I. Akbas, and D. Turgut, "A mobility model of theme park visitors," *IEEE Transactions on Mobile Computing*, vol. 14, no. 12, pp. 2406–2418, Dec 2015.

[37] X. Kang, L. Liu, H. Ma, and D. Zhao, "Urban context aware human mobility model based on temporal correlation," in *2017 IEEE International Conference on Communications (ICC)*, May 2017, pp. 1–6.

[38] A. Mei and J. Stefa, "SWIM: A simple model to generate small mobile worlds," in *IEEE INFOCOM 2009*, April 2009, pp. 2106–2113.

[39] Q. Zheng, X. Hong, J. Liu, D. Cordes, and W. Huang, "Agenda driven mobility modelling," *Int. J. Ad Hoc Ubiquitous Comput.*, vol. 5, no. 1, pp. 22–36, Dec. 2010.

[40] U. S. D. O. Transportation and F. H. Administration, "2001 national household travel survey," URL, 2007. [Online]. Available: http://nhts.ornl.gov

[41] J. Ghosh, S. J. Philip, and C. Qiao, "Sociological orbit aware location approximation and routing (SOLAR) in MANET," *Ad Hoc Networks*, vol. 5, no. 2, pp. 189–209, 2007.

[42] V. Borrel, F. Legendre, M. D. de Amorim, and S. Fdida, "SIMPS: Using sociology for personal mobility," *IEEE/ACM Transactions on Networking*, vol. 17, no. 3, pp. 831–842, June 2009.

[43] S. Yang, X. Yang, C. Zhang, and E. Spyrou, "Using social network theory for modeling human mobility," *IEEE Network*, vol. 24, no. 5, pp. 6–13, September 2010.

[44] M. Ahmed, S. Goyal, S. Singh, and J. Gupta, "An improved Spray and Wait routing protocol for Delay Tolerant Network," in *2019 2nd IEEE Middle East and North Africa COMMunications Conference (MENACOMM)*, 2019, pp. 1–6.

[45] J. Wu, M. Xiao, and L. Huang, "Homing spread: Community home-based multi-copy routing in mobile social networks," in *Proceedings of 2013 Proceedings IEEE INFOCOM*, April 2013, pp. 2319–2327.

[46] F. Khadar and T. Razafindralambo, "Performance evaluation of gradient routing strategies for wireless sensor networks," in *Proceedings of International Conference on Research in Networking*. Springer, 2009, pp. 535–547.

[47] N.-C. Wang, J.-S. Chen, Y.-F. Huang, S.-M. Wang, and S. Chen, "A Greedy Location-Aided Routing Protocol for Mobile Ad Hoc Networks," in *Proceedings of WSEAS International Conference. Proceeding. Mathematics and Computers in Science and Engineering*, no. 8, 2009.

[48] A. N. Abdajbar, K. S. Mohamed, and M. Y. Alias, "Link Budget Based Optimised Link State Routing Protocol in Flying Ad-hoc Networks," in *2019 IEEE Conference on Sustainable Utilization and Development in Engineering and Technologies (CSUDET)*, 2019, pp. 261–264.

[49] R. Arnous, E.-S. M. T. El-kenawy, and M. Saber, "A Proposed Routing Protocol for Mobile Ad Hoc Networks," *International Journal of Computer Applications*, vol. 975, p. 8887, 2019.

[50] E. Bulut and B. K. Szymanski, "Exploiting Friendship Relations for Efficient Routing in Mobile Social Networks," *IEEE Transactions on Parallel and Distributed Systems*, vol. 23, no. 12, pp. 2254–2265, Dec 2012.

[51] P. Hui, J. Crowcroft, and E. Yoneki, "BUBBLE Rap: Social-Based Forwarding in Delay-Tolerant Networks," *IEEE Transactions on Mobile Computing*, vol. 10, no. 11, pp. 1576–1589, Nov 2011.

[52] F. Li, H. Jiang, H. Li, Y. Cheng, and Y. Wang, "SEBAR: Social-Energy-Based Routing for Mobile Social Delay-Tolerant Networks," *IEEE Transactions on Vehicular Technology*, vol. 66, no. 8, pp. 7195–7206, Aug 2017.

[53] H. Lenando and M. Alrfaay, "Epsoc: Social-based epidemic-based routing protocol in opportunistic mobile social network," *Mobile Information Systems*, 2018.

[54] N. Raghav and A. Kumar, "Routing Strategy based on Centrality in Opportunistic Networks," in *2019 6th International Conference on Computing for Sustainable Global Development (INDIACom)*, 2019, pp. 922–926.

[55] J. Yim, H. Ahn, and Y.-B. Ko, "The betweenness centrality based geographic routing protocol for unmanned ground systems," in *Proceedings of the 10th International Conference on Ubiquitous Information Management and Communication*, 2016, pp. 1–4.

[56] G. Wang, L. Zheng, L. Yan, and H. Zhang, "Probabilistic routing algorithm based on transmission capability of nodes in DTN," in *Proceedings of 2017 11th IEEE International Conference on Anti-counterfeiting, Security, and Identification*, Oct 2017, pp. 146–149.

[57] N. Vanitha *et al.*, "Binary Spray and wait routing Protocol with controlled replication for DTN based Multi-Layer UAV Ad-hoc network Assisting VANET," *Turkish Journal of Computer and Mathematics Education (TURCOMAT)*, vol. 12, no. 10, pp. 276–2782, 2021.

[58] Y. Kuronuma, H. Suzuki, and A. Koyama, "An Adaptive DTN Routing Protocol Considering Replication State," in *Proceedings of 2017 31st International Conference on*

Advanced Information Networking and Applications Workshops, March 2017, pp. 421–426.

[59] H. Kaur and H. Kaur, "An enhanced spray-copy-wait dtn routing using optimized delivery predictability," in *Computer Communication, Networking and Internet Security*. Springer, 2017, pp. 603–610.

[60] Eung-Hyup Kim, Jae-Choong Nam, Jae-In Choi, and You-Ze Cho, "Probability-based spray and wait protocol in Delay Tolerant Networks," in *Proceedings of The International Conference on Information Networking 2014*, Feb 2014, pp. 412–416.

[61] A. Socievole, E. Yoneki, F. De Rango, and J. Crowcroft, "ML-SOR: Message routing using multi-layer social networks in opportunistic communications," *Computer Networks*, vol. 81, pp. 201–219, 2015.

[62] F. De Rango, A. Socievole, and S. Marano, "Exploiting online and offline activity-based metrics for opportunistic forwarding," *Wireless Networks*, vol. 21, no. 4, pp. 1163–1179, 2015.

[63] S. Kullback and R. A. Leibler, "On information and sufficiency," *The Annals of Mathematical Statistics*, vol. 22, no. 1, 1951.

[64] F. J. Massey Jr, "The kolmogorov-smirnov test for goodness of fit," *Journal of the American statistical Association*, vol. 46, no. 253, pp. 68–78, 1951.

[65] N. Duffield, C. Lund, and M. Thorup, "Estimating flow distributions from sampled flow statistics," *IEEE/ACM Transactions on Networking*, vol. 13, no. 5, pp. 933–946, 2005.

[66] K. P. Burnham and D. R. Anderson, "Multimodel inference: Understanding AIC and BIC in model selection," *Sociological Methods & Research*, vol. 33, no. 2, pp. 261–304, 2004.

[67] D. J. MacKay, *Information theory, inference and learning algorithms*. Cambridge university press, 2003.

[68] J. Pfanzagl, *Parametric statistical theory*. Walter de Gruyter, 1994.

[69] U. von Luxburg, "A tutorial on spectral clustering," *Statistics and Computing*, vol. 17, no. 4, pp. 395–416, Dec. 2007.

[70] J. MacQueen *et al.*, "Some methods for classification and analysis of multivariate observations," in *Proceedings of the fifth Berkeley symposium on mathematical statistics and probability*, vol. 1, no. 14. Oakland, CA, USA, 1967, pp. 281–297.

[71] A. Y. Ng, M. I. Jordan, and Y. Weiss, "On spectral clustering: Analysis and an algorithm," in *Advances in Neural Information Processing Systems*, 2002, pp. 849–856.

[72] K. Lee, S. Hong, S. J. Kim, I. Rhee, and S. Chong, "Demystifying levy walk patterns in human walks," *CSC, NCSU, Tech. Rep.*, 2008.

[73] R. W. Bohannon and A. W. Andrews, "Normal walking speed: a descriptive meta-analysis," *Physiotherapy*, vol. 97, no. 3, pp. 182–189, 2011.

[74] E. Bulut and B. K. Szymanski, "Exploiting friendship relations for efficient routing in mobile social networks," *IEEE Transactions on Parallel and Distributed Systems*, vol. 23, no. 12, pp. 2254–2265, Dec 2012.

[75] F. Li and J. Wu, "Localcom: A community-based epidemic forwarding scheme in disruption-tolerant networks," in *2009 6th Annual IEEE Communications Society Conference on Sensor, Mesh and Ad Hoc Communications and Networks*, June 2009, pp. 1–9.

[76] Maanmittauslaitos, "The national land survey of finland topographic database 03/2019," 2019.

[77] E. W. Dijkstra, "A note on two problems in connexion with graphs," *Numerische Mathematik*, vol. 1, no. 1, pp. 269–271, Dec 1959.

[78] A. Keränen, J. Ott, and T. Kärkkäinen, "The ONE Simulator for DTN Protocol Evaluation," in *SIMUTools '09: Proceedings of the 2nd International Conference on Simulation Tools and Techniques*. New York, NY, USA: ICST, 2009.

[79] D. Van Anh Duong and S. Yoon, "SRMM: A social relationship-aware human mobility model," *Electronics*, vol. 9, no. 2, p. 221, 2020.

[80] R. W. Bohannon and A. W. Andrews, "Normal walking speed: a descriptive meta-analysis," *Physiotherapy*, vol. 97, no. 3, pp. 182–189, 2011.

[81] D. Bonino, M. T. D. Alizo, C. Pastrone, and M. Spirito, "Wasteapp: Smarter waste recycling for smart citizens," in *2016 International Multidisciplinary Conference on Computer and Energy Science (SpliTech)*. IEEE, 2016, pp. 1–6.

[82] N. Basta, A. ElNahas, H. P. Grossmann, and S. Abdennadher, "A Framework for Social Tie Strength Inference in Vehicular Social Networks," in *2019 Wireless Days (WD)*, 2019, pp. 1–8.

[83] C. Li, F. Jiang, X. Wang, and B. Shen, "Optimal relay selection based on social threshold for D2D communications underlay cellular networks," in *2016 8th International Conference on Wireless Communications Signal Processing (WCSP)*, 2016, pp. 1–6.

[84] S. Moradi, J. B. Mohasefi, and E. Mahdipour, "MSN-CDF: New community detection framework to improve routing in mobile social networks," *International Journal of Communication Systems*, p. e4989, 2021.

[85] P. A. Gagniuc, *Markov chains: from theory to implementation and experimentation.* John Wiley & Sons, 2017.

[86] J. Shi, C. Qiao, D. Koutsonikolas, and G. Challen, "CRAWDAD dataset buffalo/phonelab-wifi (v. 2016-03-09)," Downloaded from https://crawdad.org/buffalo/phonelab-wifi/20160309, Mar. 2016.

[87] J. Shi, L. Meng, A. Striegel, C. Qiao, D. Koutsonikolas, and G. Challen, "A walk on the client side: Monitoring enterprise Wifi networks using smartphone channel scans," in *IEEE INFOCOM 2016 - The 35th Annual IEEE International Conference on Computer Communications*, 2016, pp. 1–9.

Author's Publications

International Journals

1. **Dat Van Anh Duong**, Seokhoon Yoon, "SRMM: A social relationship−aware human mobility model," *Electronics*, vol. 9, no. 2, p.221, Feb. 2020.

2. **Dat Van Anh Duong**, Dae−Young Kim, Seokhoon Yoon, "TSIRP: A temporal social interactions−based routing protocol in opportunistic mobile social networks," *IEEE Access*, vol. 9, pp. 72712-72729, May. 2021.

3. **Dat Van Anh Duong**, Seokhoon Yoon, "A Human Location Prediction−Based Routing Protocol in Mobile Crowdsensing−Based Urban Sensor Networks," *Applied Sciences*, vol. 12, no. 8, p.3898, Apr. 2022.

Domestic Journals

1. **Dat Van Anh Duong**, Seokhoon Yoon, "A Human Mobility Model in Shipyards," *International Journal of Internet, Broadcasting and Communication*, vol. 12, no. 4, pp.93-101, Nov. 2020.

2. **Dat Van Anh Duong**, Seokhoon Yoon, "A Human Movement Stream Processing System for Estimating Worker Locations in Shipyards," *International Journal of Internet, Broadcasting and Communication*, vol. 13, no. 4, pp.135-142, Nov. 2021.

International Conferences

1. **Dat Van Anh Duong**, Seokhoon Yoon, "A Social Relationship-aware Mobility Model," in *Proc. 2018 IEEE 4th World Forum on Internet of Things (WF-IoT)*, pp.658-663, Feb. 2018, Singapore, Singapore.

2. **Dat Van Anh Duong**, Seokhoon Yoon, "An Efficient Probabilistic Routing Algorithm based on Limiting the Number of Replications," in *Proc. 2019 International*

Conference on Information and Communication Technology Convergence (ICTC), pp.562-564, Oct. 2019, Jeju, Korea.

3. **Dat Van Anh Duong**, Seokhoon Yoon, "A Human Mobility Model in Malls," in *Proc. 2020 International Conference on Information and Communication Technology Convergence (ICTC)*, pp.562-564, Oct. 2020, Jeju, Korea.

Domestic Conferences

1. **Dat Van Anh Duong**, Seokhoon Yoon, "A Workflow-based Mobility Model of Workers in Shipyards," in *Proc. The Korean Institute of Communications and Information Sciences Summer Conference 2021*, pp.1011-1012, Jun. 2021, Jeju, Korea.

2. Quan T.Ngo, **Dat Van Anh Duong**, Doi Thi Lan, Seokhoon Yoon, "Estimating Workers' Locations in Industrial Sites," in *Proc. The Korean Institute of Communications and Information Sciences Fall Conference 2021*, pp.239-240, Nov. 2021, Yeosu, Korea.